Sea ice variations and trends during the Common Era in the Atlantic sector of the Arctic Ocean

Ana Lúcia Lindroth Dauner[1], Frederik Schenk[2,3,4], Katherine Elizabeth Power[3,5], Maija Heikkilä[1,6]

[1]Environmental Change Research Unit (ECRU), Ecosystems and Environment Research Programme, Faculty of Biological and Environmental Sciences, University of Helsinki, Helsinki, 00014, Finland
[2]Department of Geosciences and Geography, University of Helsinki, Helsinki, 00014, Finland
[3]Bolin Centre for Climate Research, Stockholm University, Stockholm, 10691, Sweden
[4]Department of Geological Sciences, Stockholm University, Stockholm, 10691, Sweden
[5]Department of Physical Geography, Stockholm University, Stockholm, 10691, Sweden
[6]Helsinki Institute of Sustainability Science (HELSUS), University of Helsinki, Helsinki, 00014, Finland

Correspondence to: Ana Lúcia Lindroth Dauner (ana.lindrothdauner@helsinki.fi; anadauner@gmail.com)

Abstract. Sea ice is crucial in regulating the heat balance between the ocean and atmosphere and quintessential for supporting the prevailing Arctic food web. Due to limited and often local data availability back in time, the sensitivity of sea-ice proxies to long-term climate changes is not well constrained, which renders any comparison with palaeoclimate model simulations difficult. Here we compiled a set of marine sea-ice proxy records with a relatively high temporal resolution of at least 100 years covering the Common Era (past 2k) in the Greenland-North-Atlantic sector of the Arctic to explore the presence of coherent long-term trends and common low-frequent variability and compared those with transient climate model simulations. We used cluster analysis and empirical orthogonal functions to extract leading modes of sea-ice variability, which efficiently filtered out local variations and improved comparison between proxy records and model simulations. We find that a compilation of multiple proxy-based sea-ice reconstructions accurately reflects general long-term changes in sea-ice history, consistent with simulations from two transient climate models. Although sea-ice proxies have varying mechanistic relationships to sea-ice cover, typically differing in habitat or seasonal representation, the long-term trend recorded by proxy-based reconstructions showed a good agreement with summer minimum sea-ice extent from the model simulations. The short-term variability was not as coherent between proxy-based reconstructions and model simulations. The leading mode of simulated sea-ice associated with the multidecadal to centennial timescale presented a relatively low explained variance and might be explained by changes in solar radiation and/or inflow of warm Atlantic waters to the Arctic Ocean. Short variations in proxy-based reconstructions, however, are mainly associated with local factors and the ecological nature of the proxies. Therefore, regional or large-scale view of sea-ice trend necessitates multiple spatially spread sea-ice proxy-based reconstructions, avoiding confusion between long-term regional trends and short-term local variability. Local-scale sea-ice studies, in turn, benefit from reconstructions from well-understood individual research sites.

Graphical Abstract
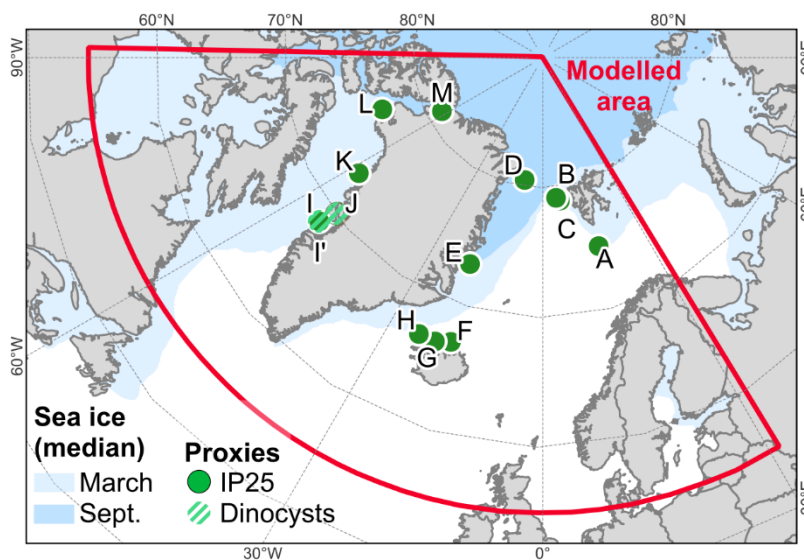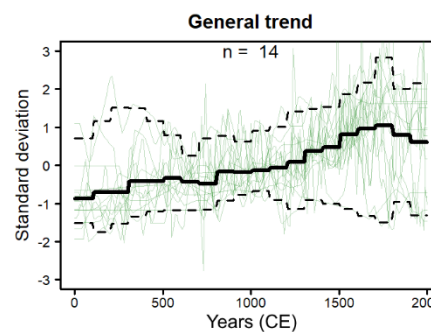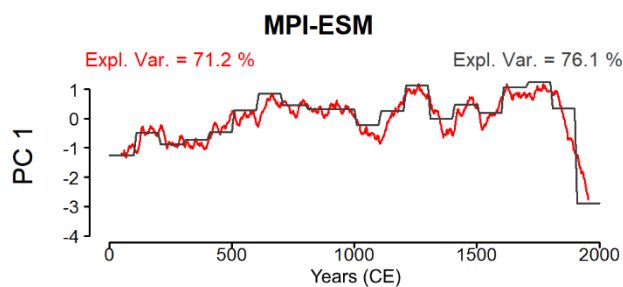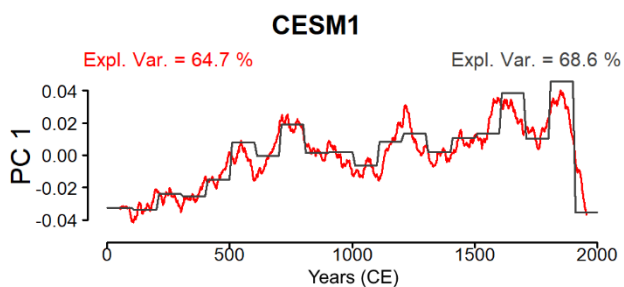
1 Introduction

Sea ice is crucial in regulating the heat balance between the ocean and the atmosphere and plays a major role in the Arctic food web (Arrigo, 2014; IPCC, 2021). Despite the importance of sea ice for ecosystems and climate, reconstructing its
40 history remains challenging (Heikkilä et al., 2022). While the development of palaeoceanographic sea-ice proxies has progressed in recent decades (de Vernal et al., 2013; Belt, 2019; Weckström et al., 2020), they often exhibit strong local and regional dependencies, limiting their use for large-scale extrapolation (Brennan and Hakim, 2022). In contrast, longer transient paleoclimate simulations of large-scale sea-ice changes using numerical models have only recently become available (Zhong et al., 2018; Mauritsen et al., 2019). Therefore, the identification and distinction between average long-term
45 trends, and regional and internally forced variability has remained a challenge.

Sea ice affects global and regional climate systems through its role in modification of water and energy budgets (Macias-Fauria and Post, 2018; Kretschmer et al., 2020; IPCC, 2021). It acts as a physical barrier, preventing heat and moisture transfers between the ocean and the atmosphere, which has significant impacts on weather and climate (Bintanja, 2018; Sun et al., 2018). Also, sea ice reflects a large part of incoming solar radiation back to space due to its high surface albedo,
50 moderating ocean warming at high latitudes (Bader et al., 2020). A reduction in high-latitude surface albedo causes a non-linear response known as Arctic amplification - a phenomenon in which northern high latitudes are warming two to four times faster than the global mean (Dai et al., 2019; Rantanen et al., 2022; Ryan et al., 2022). In addition to being a key climate parameter, sea ice presence is fundamental to Artic marine ecosystems. Sea ice provides a unique habitat for diverse biological communities formed by ice-dwelling (sympagic) and ice-dependent species (Eamer et al., 2013; Arrigo, 2014).
55 While multiyear sea ice provides a year-round habitat that supports endemic Arctic species, areas seasonally covered by sea ice have the highest marine primary production by ice algal and phytoplankton blooms during the melt and open-water seasons (Hop and Gjøsæter, 2013; Lannuzel et al., 2020).

A major challenge for comprehending the consequences of present climate change on sea ice and Arctic marine ecosystems, is the lack of baseline data (Heikkilä et al., 2022). Most human observations of sea ice are derived from satellites and date
60 back only to the 1970s (Fox-Kemper et al., 2021). Palaeoclimate data derived from marine sediments can provide insights into Arctic environmental change over much longer time scales. However, most Arctic palaeoclimate data compilations so far have focused on past temperatures and the majority of the compiled data originates in terrestrial environments. For example, McKay and Kaufman (2014) compiled 56 records in an Arctic proxy temperature database for the past 2000 years, but only six record ocean temperatures. More recently, a global temperature reconstruction for the Common Era (CE)
65 compiled more than 200 proxy records but none of the marine-related reconstructions were located in the Arctic Ocean (PAGES 2k Consortium, 2019).

To our knowledge, there are only two proxy-based data compilations of past sea-ice cover (Kinnard et al., 2011; Brennan and Hakim, 2022), neither of which focuses on marine sea-ice proxies. Kinnard et al. (2011) reconstructed sea-ice conditions over the past 1450 years using ice-core records, tree-ring chronologies and lake sediments. Brennan and Hakim (2022)

70   assimilated temperature-sensitive proxy records from tree rings, ice cores, corals, lake sediments and bivalve records into a numerical model to study Arctic sea-ice conditions during the Common Era. However, a wealth of evidence of past sea-ice evolution during the Common Era have been made using sea-ice proxies preserved in marine sediments, typically microfossil assemblages (e.g. Sha et al., 2017; Tsoy et al., 2017; Allan et al., 2018) and source-specific algal lipids (e.g. Belt et al., 2010; Cabedo-Sanz et al., 2016; Detlef et al., 2021). Past sea-ice reconstructions based on microfossils rely on the

75   presence and abundance of species associated with the presence of seasonal sea ice, typically diatoms or resting stages (cysts) of dinoflagellates (de Vernal et al., 2013; Weckström et al., 2020). Highly branched isoprenoid lipids (HBIs) linked with sea-ice environments are increasingly common in sea-ice reconstructions, in particular IP_{25} ("Ice Proxy with 25 carbon atoms"). It is produced by a few strictly sympagic diatoms, and has a strong link to seasonal sea-ice presence and concentration (Belt, 2019). Although the use of sea-ice proxies is becoming more widespread, local and regional forcings

80   such as nutrient availability, freshwater and sediment contributions from land might affect the organisms whose sedimentary remains are used in sea-ice reconstructions (Brown et al., 2020; Luostarinen et al., 2020, 2023; Marret et al., 2020). Therefore, individual sea-ice reconstructions likely incorporate noise from local sea-ice characteristics and forcings other than regional-scale sea-ice cover. There are studies integrating multiple sampling sites or sediment cores, often describing and visually comparing sea-ice evolution among the records (e.g. de Vernal et al., 2013; Maffezzoli et al., 2021). However,

85   an integration of existing sea-ice reconstructions in a systematic way to underline main trends and/or variability has, so far, not been undertaken.

Combining proxy data synthesis with climate model outputs may allow to distinguish local sea-ice changes from large-scale variability, complementing and strengthening the interpretation of past sea-ice evolution (Moffa-Sánchez et al., 2019; Brennan and Hakim, 2022). In contrast to proxies, numerical models offer improved spatial coverage and temporal

90   resolution and can provide a coherent and physically consistent overview of the climate on varying timescales, although large model biases exist in Arctic regions, attributable to complex feedback framework (Goosse et al., 2013, 2018). Though the majority of simulations contributing to the latest Coupled Model Intercomparison Project (CMIP6) included sea ice as a variable, detailed evaluations of sea ice in paleoclimate simulations are still pending, as long transient simulations and more sea-ice proxies have become available only recently (Zhong et al., 2018; Mauritsen et al., 2019).

95   Here, we use high-resolution sea-ice reconstructions based on palaeoceanographic proxies together with numerical model outputs to identify possible common trends and/or regional differences in the evolution of sea-ice cover over the Common Era in the Atlantic sector of the Arctic Ocean. We also aim to probe whether sea-ice proxies (microfossils and IP_{25}) are suited to capture large-scale sea-ice changes or if local forcings have a larger influence. Lastly, we discuss the external forcings that may be causing the sea-ice changes observed in our study.

2 Material and Methods

2.1 Data

Palaeoceanographic datasets were obtained from the databases by NOAA (https://www.ncei.noaa.gov/access/paleo-search/), PANGAEA (https://www.pangaea.de/) and Neotoma (https://www.neotomadb.org/) between January and June 2021. Additional published records were solicited from the original authors. Based on the availability of suitable records, we focused on sediment cores retrieved from high latitudes (> 55° N) and the Atlantic sector of the Arctic Ocean (90° W to 30° E) that covered at least 80% of the CE and presented an average temporal resolution < 100 years.

The search included data of concentrations of highly branched isoprenoid lipid IP_{25} (Ice Proxy with 25 carbon atoms) derived from sympagic algae, the abundance of diatom indicator species (*Fragilariopsis cylindrus*, *F. oceanica*, *F. reginae-jahniae* and *Fossulaphycus arcticus*) and the abundance of dinoflagellate cyst indicator species (*Islandinium minutum* and *I.? cezare*).

The biogeochemical proxy IP_{25} was chosen due to its source-selectivity, as it is produced only by certain sympagic diatoms that are common across the Arctic Ocean (Belt, 2018). This lipid is produced in the ice during the sympagic spring bloom prior to ice melt, and is, therefore, interpreted as a proxy measure of seasonal sea ice. Since IP_{25} is not produced in ice-free areas or under permanent/extensive sea-ice cover due to light limitation, changes in its concentration are interpreted in terms of fluctuations in seasonal sea-ice extent (Belt, 2019).

Microfossils of sympagic diatoms are typically not found in sediments (Limoges et al., 2018; Luostarinen et al., 2023). Thus, the diatom indicator species for sea-ice are those that bloom in abundance under the ice or at the ice edge during spring melt. These species can be found in small concentrations within the ice matrix, indicating blooms seed in the ice matrix, while their main occurrence is in the stratified waters in the marginal ice zone. *Fossulaphycus arcticus*, *F. reginae- jahniae* and *F. oceanica* present a significant relationship with high April sea-ice concentrations in the Atlantic Arctic (Weckström et al., 2020). On the other hand, although *F. cylindrus* has been frequently used as a sea-ice indicator, it is also commonly found in cold-water ice-free regions and/or periods (Luostarinen et al., 2020; Weckström et al., 2020). Nevertheless, *F. cylindrus* regularly occurs in the marginal ice zone and dominates exported material to the sediments during the melt season (Oksman et al., 2019; Luostarinen et al., 2023).

The dinoflagellate cyst indicator species *Islandinium minutum* and *I.? cezare* were also chosen due to their affinity with seasonally sea-ice covered regions. They are found most abundantly in surface sediments in Arctic areas that experience seasonal sea ice and are mainly associated with cold waters from polar to subpolar regions (Head et al., 2001; de Vernal et al., 2020). Their ecological connection to sea-ice cover is, however, unresolved. Recently, for example, Luostarinen et al. (2023) observed that these species were virtually absent in sea ice, water column and sediment flux during spring melt although being common in surface sediments.

Concentration data were obtained in the form of mass of IP_{25} either related to sediment dry weight (µg/g dw or ng/g dw) or normalized by total organic carbon (µg/g TOC or ng/g TOC). When available, we analysed the data normalized by TOC, to

correct for changes in sedimentation rates. Diatom and dinoflagellate cyst abundance data were retrieved as indicator species proportion (%) of the total species assemblage. We decided to focus only on measured proxy concentrations and abundances

135 instead of quantitatively estimates of reconstructed sea-ice concentrations and sea-ice duration. This is because quantitative reconstructions incorporate species assemblages, including taxa not related to sea ice and primarily controlled by other environmental factors. Furthermore, the mechanistic relationships of many of the proxies to the reconstructed environmental parameter are still not thoroughly understood (Heikkilä et al., 2022). Importantly, while each proxy record used here is based on measured quantities, the proxies represent a relative measure of seasonal sea-ice concentrations rather than geophysical

140 quantities.

The chronologies were based on radiocarbon dating (AMS ^{14}C), and the age-depth models from the original authors were used.

2.2 Numerical models

Two climate simulations covering the past 2000 years (2k) were used. These are the Max Planck Institute Earth system

145 model 1.2 Low Resolution (MPI-ESM1.2-LR; hereafter MPI-ESM) (Mauritsen et al., 2019) which was used to perform past 2k transient simulations (Jungclaus et al., 2017; van Dijk et al., 2022), and the Community Earth System Model 1.1 (CESM1.1/CCSM4; hereafter CESM1) past2k transient simulation (Zhong et al., 2018). Both models contributed to the PMIP (Paleoclimate Model Intercomparison Project) part of the Coupled Model Intercomparison Project Phase 6 (CMIP6) (Jungclaus et al., 2017).

150 The MPI-ESM consists of four model components: ocean dynamical model MPIOM1.6, ocean biogeochemistry model HAMOCC6, atmosphere model ECHAM6.3 and land model JSBACH3.2. These are coupled together via the OASIS3-MCT coupler. The configuration used is ~150 km in the ocean and ~200 km in the atmosphere, with 47 atmospheric vertical levels (Mauritsen et al., 2019). CESM1 is also a global fully coupled model consisting of 4 component models: atmospheric model (AGCM), ocean model (OGCM), land surface model (CLM) and sea ice model (CICE) connected by a central coupler

155 (Craig et al., 2012). It has a ~1° resolution in the ocean and sea ice and ~2° resolution in the atmosphere (Zhong et al., 2018). Both simulations are transient, meaning they start from past climate boundary conditions, but the exact starting time varies. They then simulate the climate forward through the past2k. Forcing data for the past2k experiments is based on the PMIP4 protocol (Jungclaus et al., 2017). For CESM1, forcings are solar irradiance and volcanic aerosols (Toohey et al., 2016), land use and land cover (Klein Goldewijk et al., 2010), and greenhouse gas levels (MacFarling Meure et al., 2006). For both

160 simulations, orbital forcing is from Berger (1978). For MPI-ESM, forcings include solar irradiance (Krivova et al., 2011), land use (Hurtt et al., 2011) and greenhouse gas levels (Brovkin et al., 2019). The only variable studied is sea ice fraction, specifically "sea ice area percentage" (Siconca) from MPI-ESM and "fraction of surface area covered by sea ice" (Icefrac) from CESM1. These represent the percentage of ice cover in each grid square and both variables are on atmospheric grids. Extra-tropical (30 – 60 °N) surface air temperature is used in addition for model comparison (Figure 4).

2.3 Statistical analyses

Maps were made using QGIS (QGIS Development Team, 2022). All statistical analyses were performed in R environment (R Core Team, 2022).

Prior to statistical analyses, all proxy datasets were standardized to allow a direct comparison among data from disparate sources. Z-scores were calculated by subtracting the data by the mean and dividing by the standard deviation of each record, considering only data dated to the Common Era. To allow statistical comparisons, all datasets were reduced to a common resolution by binning to the same 100-year time slices (the top sample, centred at 1950 AD, integrated the time slice 1900 – 2000 AD, and so on) (Shuman et al., 2018).

A cluster analysis using SAX representation (Lin et al., 2007) in the dissimilarity measure calculation was used to categorize the marine proxy records into groups according to their evolution through time. SAX representation is a "structured-based" dissimilarity measure that focuses on comparing underlying dependence structures and is thus suitable for time-series analyses. The symbolization approach involves transformation of time series into sequences of discretized symbols, allowing dimensionality reduction but keeping the distance measures defined on the original time series (Lin et al., 2007). Thus, this approach can be used to group different proxy records according to their temporal evolution, regardless of their units. The cluster analysis was repeated using the globally (over all used records) detrended records to remove the overall dominant influence of the global trend. For this, we calculate the average of each time step of the z-score records (the global trend) and subtracted this average from each of the z-score records. Finally, the data pertaining to each group were averaged, in order to create a unique record for each group. The TSclust package (Montero and Vilar, 2014) was used to run the cluster analyses and the zoo package (Zeileis et al., 2022) was used to deal with the missing values.

For the exploration of the climate models, we used annual sea-ice minimum and maximum of monthly mean data. Sea-ice extents (km^2) were calculated by multiplying the sea ice fraction in each grid (%) by its grid area (km^2) and summing the area of all grids which gives the annual extent. For better visualization, the data was smoothed with a 100-year running mean. To mimic the behaviour of our proxy records, we repeated the analysis using 100-years mean chunks e.g., for the EOF analysis. Pearson correlation analysis were calculated between sea-ice extents from the whole Arctic Ocean and from the area around Greenland using the package Hmisc (Harrell Jr., 2022).

All model data was filtered using a low-pass red noise Butterworth filter to remove sub-decadal oscillations using the signal package (Ligges et al., 2022). A wavelet analysis (Morlet wavelet) was performed using the sea ice extents (annual resolution) to identify significant oscillations that could show coherence between different datasets or represent unforced variations, using the WaveletComp package (Roesch and Schmidbauer, 2018). Additionally, we applied an empirical orthogonal function (EOF) analysis for the unfiltered sea ice fraction data to identify the main modes of variability and their spatial representation. Prior to EOF analysis, we applied a log-transformation of the fractional data using log10 after adding an arbitrary offset of 0.5 to avoid zeroes. In order to test the applicability of the 100-year time slices used for the proxy data, we calculated the EOFs using annual data, the 100-year running mean and the 100-year mean chunks. They all presented

similar results, considering both EOF1/2 and PC1/2, and in this study we are presenting EOFs and PCs based on the smoothed 100-year running mean data and also the PCs based on the 100-year time-slices. EOFs were calculated with CDO

200   version 1.9.10 (Schulzweida, 2021).

Other packages used during the analyses were dplyr (Wickham et al., 2022) to clean and organize the data, and ncdf4 (Pierce, 2015) to import the files produced by CDO into R.

3 Results and Discussion

3.1 Proxy-based sea-ice reconstructions

205   Based on our spatial, temporal and resolution criteria, we retrieved 14 sea-ice reconstructions from 13 different sites (Figure 1, Table 1). Twelve of them were based on IP_{25} concentrations and two were based on dinocyst assemblages. Unfortunately, there were no sea-ice records based on diatoms fitting our criteria of sufficient time coverage and resolution, and geographical boundaries.

210   **Table 1. Marine record data including latitude, longitude, water depth and analysed variables.**

Record	Core	Region	Latitude	Longitude	Water Depth (m)	Variable	Reference
A	JM09-KA11-GC	Barents Sea	74.87482	16.48482	345	IP_{25}	Köseoğlu et al., 2018
B	MSM05/5_712-1	Fram Strait	78.91567	6.76733	1490	IP_{25}	Cabedo-Sanz and Belt, 2016
C	MSM05/5_723-2	Fram Strait	79.16100	5.33783	1349	IP_{25}	Müller et al., 2012
D	PS93/025-1/2	Fram Strait	80.48117	-8.48867	290	IP_{25}	Syring et al., 2020
E	PS2641-4/5	Greenland Sea	73.15500	-19.48500	469	IP_{25}	Kolling et al., 2017
F	JR51-GC35	Denmark Strait	66.99933	-17.96100	420	IP_{25}	Cabedo-Sanz et al., 2016
G	MD99-2269	Denmark Strait	66.62550	-20.85267	365	IP_{25}	Cabedo-Sanz et al., 2016
H	MD99-2263	Denmark Strait	66.67900	-24.19600	235	IP_{25}	Andrews et al., 2009
I	MSM05/3_343310-5-1	Baffin Bay	68.64768	-53.82488	855	IP_{25}	Kolling et al., 2018
I'	MSM05/3_343310-5-1	Baffin Bay	68.64768	-53.82488	855	dinocyst	Allan et al., 2018
J	DA06-139G	Baffin Bay	70.09143	-52.89308	384	dinocyst	Andresen et al., 2011
K	AMD14-204_CASQ	Baffin Bay	73.26105	-57.89978	987	IP_{25}	Limoges et al., 2020
L	AMD16-117Q	Baffin Bay	77.00483	-72.13867	964	IP_{25}	Jackson et al., 2021
M	OD1507 (composite 03TC-41GC-03PC)	Arctic Ocean	81.19133	-62.03767	976	IP_{25}	Detlef et al., 2021
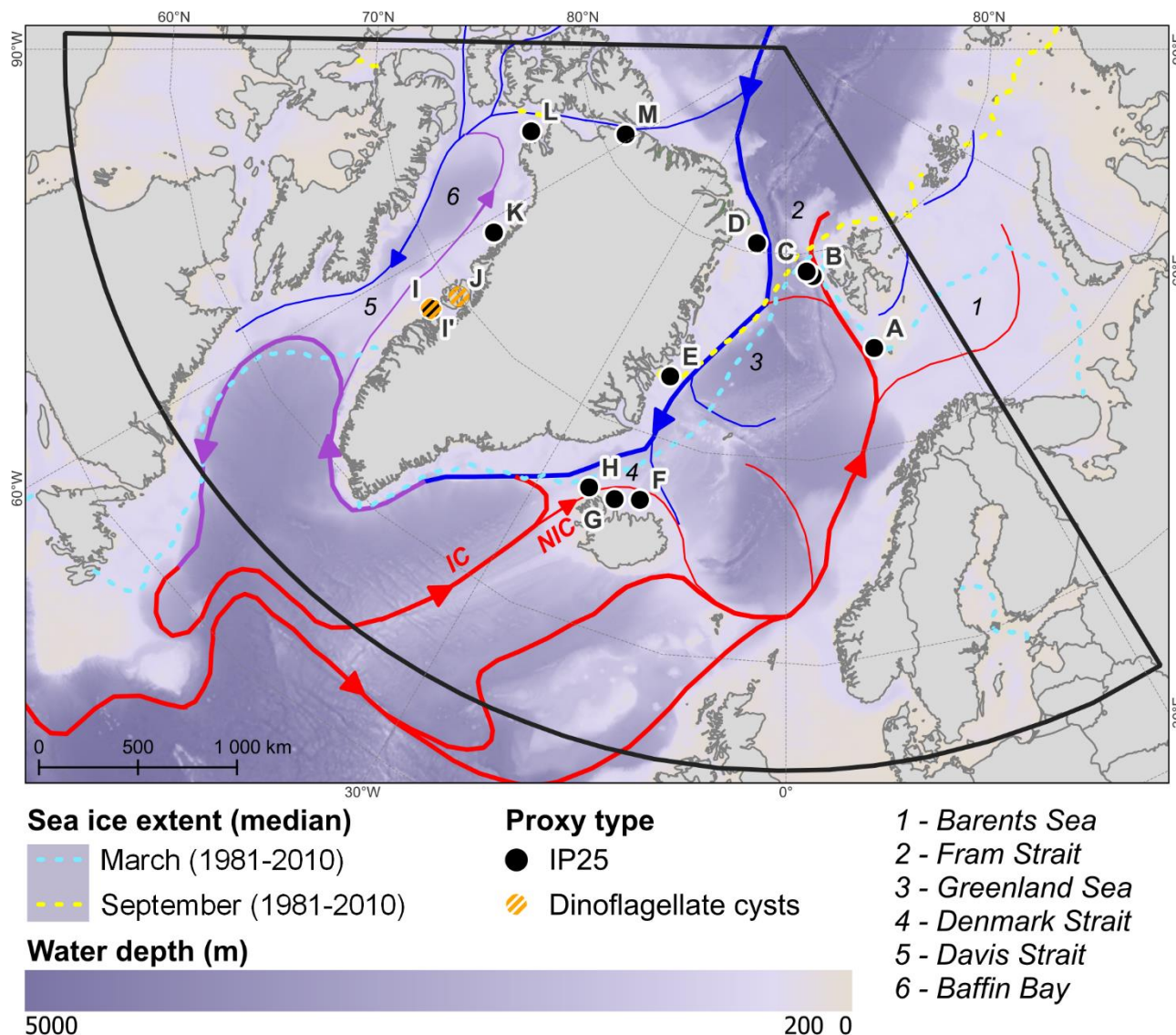
Figure 1. Map showing the locations of IP$_{25}$ and dinoflagellate cyst records for sea-ice reconstructions. The major surface currents are shown (blue: cold waters; purple: mixed water; red: warm waters), but only the currents discussed in the text are identified. IC: Irminger current; NIC: North Irminger Current. The bold black line indicates the area used for the numerical model calculations.

215

When dealing with individual sedimentary records, increases in IP$_{25}$ concentrations and in dinoflagellate indicator species are associated with regional increases in the presence of seasonal sea-ice cover (de Vernal and Marret, 2007; Belt and Müller, 2013). Similarly, in this case, we assumed that increases observed in the temporal reconstruction for each cluster group refer to increases in sea-ice cover. For the temporal reconstruction of the cluster groups to present an increase in the z-

220

scores, this increase must have been observed in the individual records, scattered in different regions of the studied area.

225   Thus, an increase in seasonal sea ice in different areas can be interpreted as an overall increase in sea-ice cover.

All sea-ice proxy records were initially clustered in the same group (Figure 2a), evidencing that all records were under the influence of the same dominant forcing, producing a common trend (Figure 2b). This overall increase in sea-ice cover agrees with the reconstructed Neoglacial cooling in the Arctic (McKay and Kaufman, 2014) and globally (PAGES 2k Consortium, 2019), especially between 1200 and 1600 CE (Figure 2b). The cooling trend and sea-ice expansion has been largely

230   explained by the decrease in the Northern Hemisphere insolation due to orbital changes (Wanner et al., 2011) (Figure 2c). In addition, the cumulative effect of large volcanic eruptions may have contributed to this long-term cooling (Büntgen et al., 2020) culminating in the Little Ice Age (LIA; 1600 – 1850 CE in the Arctic; Wang et al., 2022) (Figure 2d). A recovery from the LIA starting around 1850 CE marks a remarkable change in the sign of trends (Figure 2b). More recently, Arctic warming and sea-ice decrease have been accelerated by anthropogenic greenhouse gas emissions and land use changes

235   (IPCC, 2021).
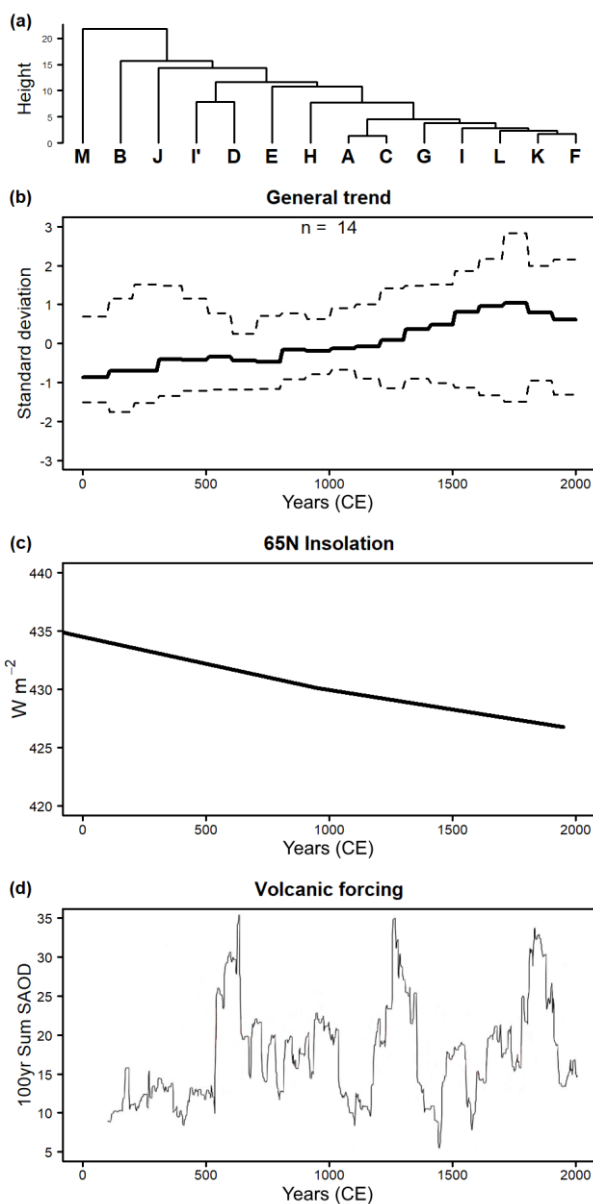
Figure 2. (a) Dendrogram and (b) average composite of the standardized sea-ice reconstructions used in this study. The solid lines represent the mean values of all records and the dashed values represent the amplitude of the standardized values. (c) Insolation at
240 **65°N from Berger and Loutre (1991). (d) Total Stratospheric Aerosol Optical Depth – SAOD from Büntgen et al. (2020). Larger SAOD values are indicative of larger volcanic dust inputs to the atmosphere.**

In addition to the common trend, the proxies presented a large variability, especially in the first and last five centuries of the

Common Era (Figure 2b). The variability observed in the sea-ice reconstructions is probably caused by other environmental

245 changes than the large-scale expansion/retraction of sea-ice cover. On both sides of Greenland, for example, the intrusion of

warm Atlantic water has been suggested as the cause of the observed short-term variability in proxy-based sea-ice records (Kolling et al., 2017; Jackson et al., 2021). Changes in the position of the atmospheric polar front (Allan et al., 2018) and interactions with ice produced within fjords (Kolling et al., 2017) have also been suggested as explanations of this variability.

250   Although all records witness a common forced trend, a large spread between the early and late part of the record indicate the presence of other local variability. To identify such second and higher order variations, we removed the common nonlinear trend from all records and repeated the cluster analysis with the now regionally detrended data. When the general trend in the proxy records was removed, three distinct groups emerge from the cluster analysis (Figure 3a). Importantly, the three groups (types of sea-ice evolution) do not form geographical entities. Instead, the sites within each group have sites located on both

255   the western and eastern side of Greenland.
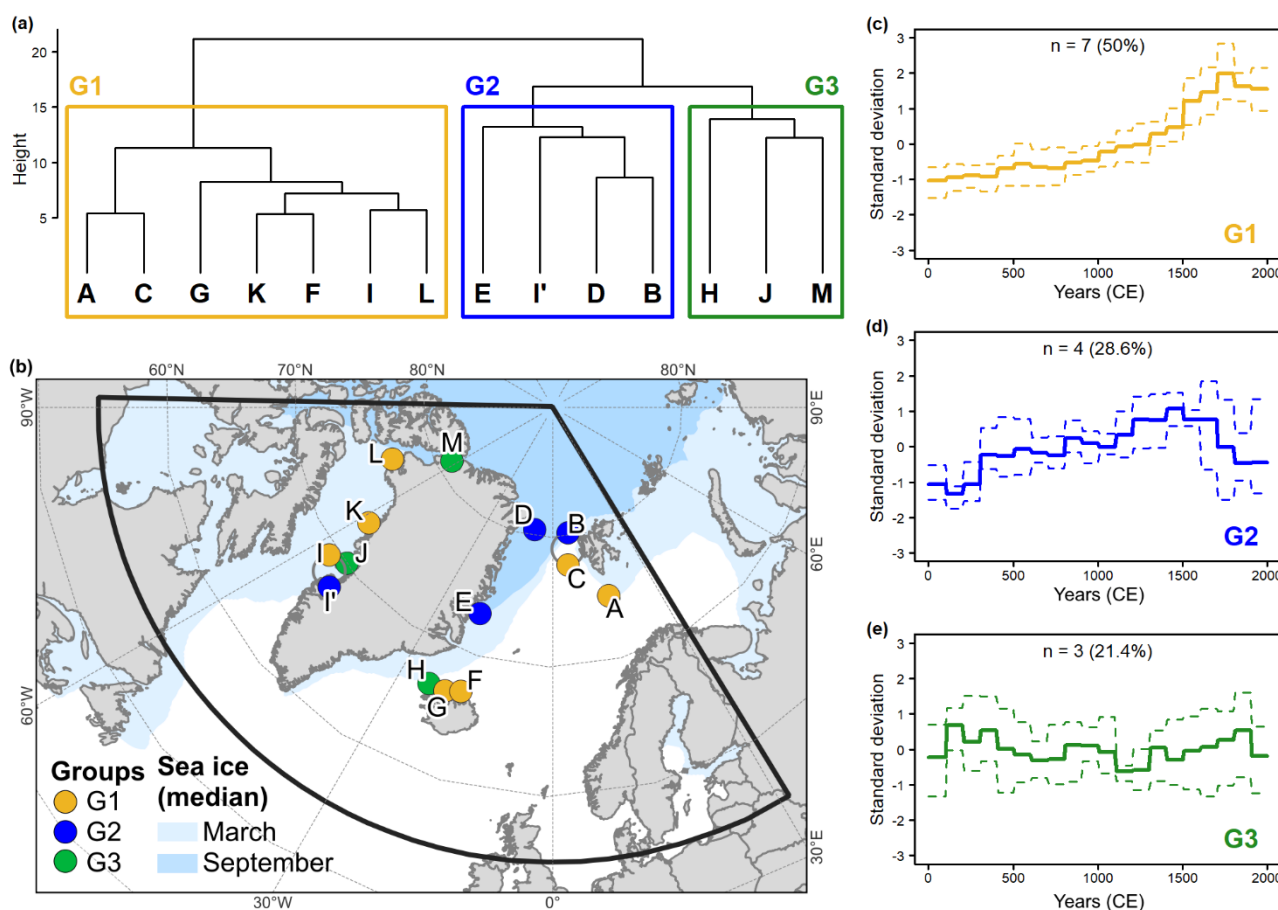
Figure 3. Dendrogram (a) and average composite (c, d, e) of the standardized sea-ice reconstructions used in this study after removing the main trend (global average). The solid lines represent the mean values of all records and the dashed values represent
260   **the amplitude of the standardized values. The spatial distribution of records in each cluster is presented in (b).**

The first group (G1, Figure 3c) presented practically the same pattern as in the general trend (Figure 2), with maximum sea-ice cover around 1750 CE, corresponding with the LIA in the Arctic (1600 – 1850 CE; Wang et al., 2022). Group 1 includes three records from Baffin Bay, two records retrieved off Svalbard and two records from northern Iceland. While Baffin Bay

265 is currently under the influence of seasonal sea-ice cover, the other four records were collected in regions south of the current winter sea-ice edge (Figure 1). The sea-ice expansion demonstrated by G1 until 1750, even after removing the general trend (Figure 2), highlights the importance of large-scale processes at these sites, such as transient changes in orbital forcing in combination with volcanism causing atmospheric cooling and consequent sea-ice expansion. Interestingly, G1 demonstrates a higher rate of sea-ice increase from 1600 CE until the LIA, which is not apparent in the general trend (Figure 2). Cabedo-

270 Sanz et al. (2016) and Miles et al. (2020) suggest that this apparent accelerating expansion of sea ice south of the Fram Strait might be caused by more sea-ice export by stronger southward currents carrying polar waters and pack ice. Thus, in addition to the sea-ice growth caused by the Neoglacial cooling, ice was also transported to more southern latitudes by stronger currents. Following the maximum sea-ice cover during the LIA, a slight decreasing trend in sea ice is demonstrated by G1. However, out of the seven records in this group, only three (A, G and L) cover the modern industrial period (after 1850 CE)

275 (Supp. Figure S1). While record G shows a decrease in the sea ice (Cabedo-Sanz et al., 2016), the other two records point to highly fluctuating sea-ice conditions (Köseoğlu et al., 2018; Jackson et al., 2021). Thus, the plateauing trend in the last century might be an artifact of the analysis, since most of the records did not have an adequate time coverage for the modern period.

Group 2 (G2; Figure 3a) is a cluster of four proxy records collected in the Fram Strait (B, D), off eastern Greenland (E) and

280 near Davis Strait, off western Greenland (I'; Figure 3b). Similar to G1, this group presented the common general trend of sea-ice expansion (Figure 2) since the beginning of the Common Era, but maximum values are reached between 1250 and 1650 CE. The similarity between G1 and G2 suggests similar internal system responses to a large-scale climate forcing. The early sea-ice maximum was followed by a sea-ice decrease, especially in the two records from Fram Strait (B and D). This decrease is probably an artifact caused by the binary behaviour of the IP_{25} proxy. While IP_{25} (produced by sympagic

285 diatoms) is absent in ice free oceans, thick, perennial sea ice also reduces sympagic diatom and thus IP_{25} production (Belt, 2018). In the original study, Cabedo-Sanz and Belt (2016) suggested that a switch from long seasonal sea-ice cover to a multiyear sea-ice scenario could explain the early decrease in IP_{25} observed in Fram Strait. Another explanation by Kolling et al. (2017) and Syring et al. (2020) also suggests colder climate but coupled to more open-water conditions due to polynya (ice free area) formation on the East Greenland shelf. It was probably caused by glacier expansion and katabatic winds

290 pushing sea ice off the coast. The sea-ice retreat observed at I´ in Davis Strait, the only G2 site in the western side of Greenland, might also be explained by the establishment of polynya conditions. The decrease in *Islandinium minutum* and *Islandinium? cezare* is concomitant with an increase in the abundances of phototrophic taxa (especially *Pentapharsodinium dalei*), potentially indicating a shift towards longer open-water seasons (Allan et al., 2018).

Interestingly, a sea-ice decrease over the last two centuries was not observed in record I, a sea-ice reconstruction from the

295   same sediment core as dinocyst record I' (MSM05/3_343310), but based on IP_{25} (Kolling et al., 2018). The differing cluster allocation of the dinocyst record (I'; G2) and the IP_{25} record (I, G3) is caused by the difference in their temporal trends and temporal coverages. Although having a good temporal resolution of 14 years, record I (IP_{25}) only covers the period until 1809 whilst record I' (dinocysts) extends to 2006 (Supp. Figures S1 and S2). Therefore, record I did not have an appropriate temporal coverage to register the potentially same decrease as observed in record I'.

300   The lack of temporal coverage is also the probable reason behind the assignments of records B and C in different groups, even though both sediment cores were retrieved from the eastern Fram Strait off Svalbard (Figure 3). While record B was assigned to Group 2 due to the decrease in IP_{25} after the 15th century (Supp. Figure S2), record C was placed in Group 1. However, record C only covers the time until 1770 CE (Supp. Figure S1). Therefore, it does not have enough temporal coverage to register a potential IP_{25} decrease.

305   Lastly, Group 3 (G3; Figure 3a) is formed by three records and presents no clear long-term trend. This group contains records that did not fit into the two previous groups rather than records with a similar sea-ice evolution. Sediment core OD1507 (composite 03TC-41GC-03PC) (record M in Figure 3b) is located inside a fjord and presents a long-term decrease in IP_{25} concentrations (Detlef et al., 2021). The authors argue that production of IP_{25} decreases with the establishment of near perennial sea-ice cover during the Common Era. Therefore, the decrease in IP_{25} is probably caused by the binary behaviour

310   of this proxy, since perennial sea ice reduces sympagic blooms and IP_{25} production (Belt, 2018). Sediment core DA06-139G (record J in Figure 3b; Supp. Figure S3) was also collected inside a strait, and was thus under the influence of land-fast sea ice and marine-terminating glaciers (Andresen et al., 2011). The lack of temporal trend might be related to the influence of freshwater coming from the continental ice sheets where atmospheric warming may increase melting and adversely cool the surface waters locally as can be observed in glacier-fed lakes during heatwaves (Kirchner et al., 2021). Limoges et al. (2018)

315   advise about the use of IP_{25} in coastal areas, as lower salinities may influence the structural nature of sea ice and its propensity to sustain algal growth. Therefore, freshwater influence might cause a decline in IP_{25}-producing diatom species.

The sediment core MD99-2263 (record H in Figure 3b), on the other hand, is located off the Iceland shelf in an open water environment and close to cores MD99-2269 (G) and JR51-GC35 (F). The main difference between records E and G (both assigned to Group 1) and record H (assigned to group 3) occurred between 1450 and 1650 (Supp. Figures S1 and S3).

320   During this period in record H, high sediment accumulation rates coincided with relatively high concentrations of IP_{25} (Andrews et al., 2009). The authors suggest that in this location the sea-ice proxy IP_{25} was associated with increasing drift ice related to changes in the wind pattern during the European LIA. Stronger N and NW winds led to more sea ice being exported from the Arctic Ocean towards the NW/N Iceland shelf. However, this increment was not as noticeable as observed in the records G and E. One possible explanation for this difference is the impact of warm waters on the melting rate of the

325   drift ice. Sediment core MD99-2263 (record H) was collected in the Denmark Strait, in a region directly under the influence of the North Irminger Current that carries warm Atlantic waters towards the Nordic Seas (Talley et al., 2011). Sediment cores MD99-2269 (G) and JR51-GC35 (F), however, are located in a more protected region off northern Iceland. Between

1450 and 1650 CE, Europe was already under the influence of LIA unlike Greenland and North America (Wang et al., 2022). The difference in the temperatures caused a strengthening of the subpolar gyre, resulting in a stronger presence of

330 warm and saline Atlantic water carried by the Irminger Current in the Denmark Strait region (Miettinen et al., 2012), where sediment core MD99-2263 (record H in Figure 3) was retrieved. Thus, it is possible that during this period, the presence of warm waters intensified the melting process of drift ice, promoting the transfer of sea ice proxies from the ocean surface to the sediments. Around 1600, the onset of LIA in Arctic and North America (Wang et al., 2022) probably caused a weakening of the Atlantic currents towards the Nordic seas.

335 **3.2 Model-based sea-ice reconstructions**

Annual mean air temperature trends (Figure 4) produced by both models in our study present a similar declining pattern as proxy-based Arctic temperatures obtained in a reconstruction by McKay and Kaufman (2014). The McKay and Kaufman (2014) reconstruction obtained a cooling of -0.49 °C/kyr for the Arctic region (latitude > 60° N) for the pre-industrial part of the Common Era (Supp. Figure S4). A comparable but less pronounced cooling is simulated by the CESM1 and MPI-ESM

340 models, with cooling rates of -0.28 and -0.21 °C/kyr, respectively (Supp. Figure S4). This implies that the reconstructed cooling trend is roughly twice as strong as in both simulations. After 1850, air temperatures present a shift towards a warming trend. In the McKay and Kaufman (2014) proxy reconstruction, the warming is 0.97 °C/100 years, while the CESM1 and MPI-ESM models yield warming rates of 1.34 and 0.84 °C/100 years, respectively (Supp. Figure S4).
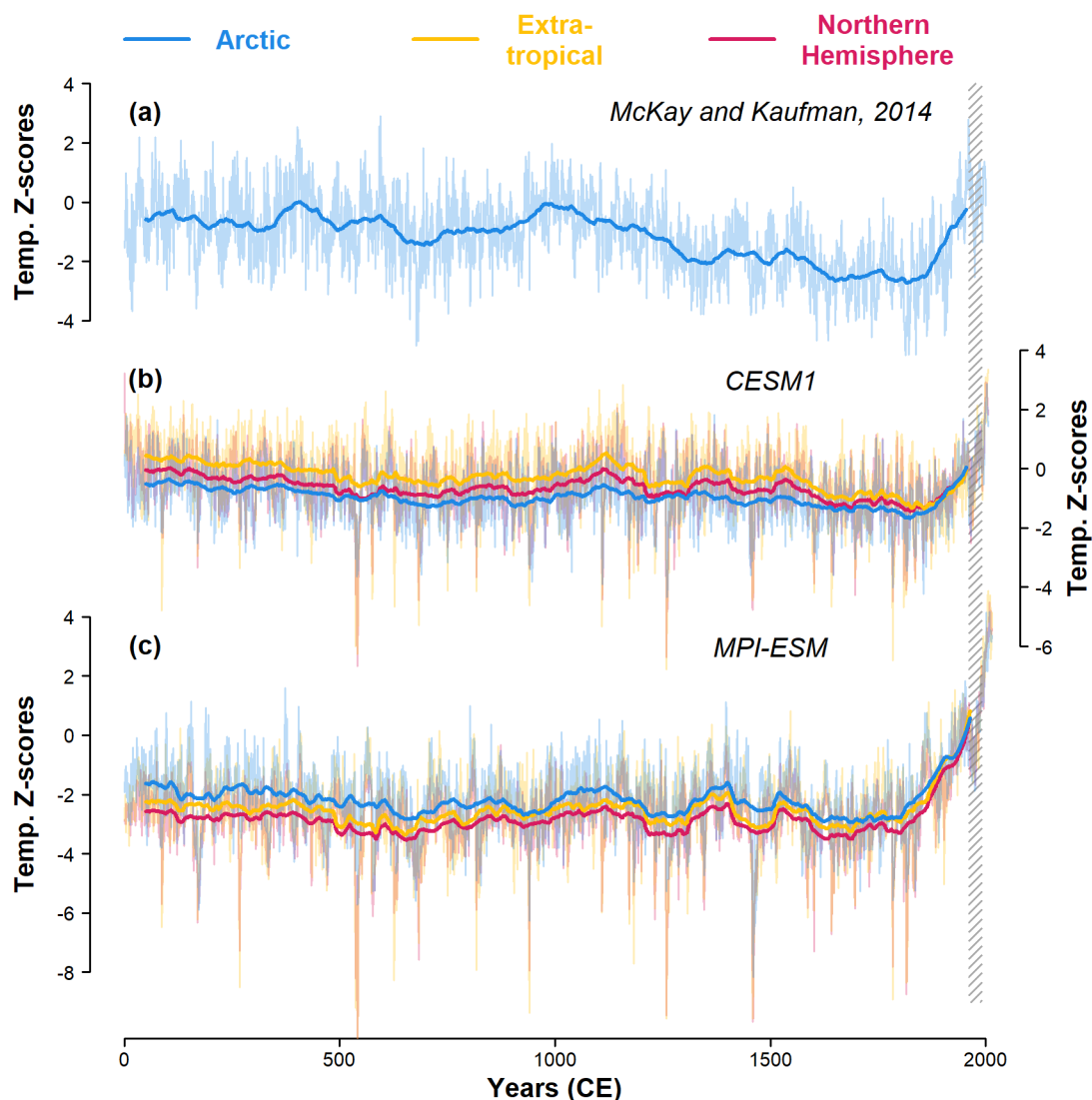
Figure 4. Air temperature *z*-scores (relative to the period between 1961-1990) based on (a) Arctic proxy data (McKay and Kaufman, 2014), (b) CESM1 simulation data and (c) MPI-ESM simulation data. Bold lines refer to 100-years running means. The hatched area indicates the period between 1961-1990. Northern Hemisphere refers to latitudes between 0 – 90° N, the Arctic region refers to latitudes between 60 – 90° N, and the Extra-tropical region refers to latitudes between 30 – 60° N.

Considering the whole Arctic region sea-ice extent from both models for the period 0 - 2000 CE, CESM 1 shows 27.4% more summer sea ice than MPI-ESM (average extents: 6.6 million km^2 vs 5.2 km^2, respectively). During winter, the difference is very small and decreases to 1.7%, with CESM1 presenting 16.1 million km^2 of average sea ice extent and MPI-ESM, 15.9 million km^2 (Table 2). There is less consistency in the region around Greenland with a strong difference during summer, with CESM 1 showing 73.4% more summer sea ice than MPI-ESM (average extents: 1.4 million km^2 vs 0.8 km^2,

respectively) (Table 2). However, disregarding the magnitude and spatial bias of the sea-ice extent, temporal changes in summer sea-ice area simulated around Greenland follow the changes as simulated for the whole Arctic Ocean (Figure 5). Considering the 100-year running mean, the correlation of annual sea-ice extent between the total Arctic Ocean and the area around Greenland is 0.92 for CESM1 and 0.93 for MPI-ESM during summer, and 0.57 for CESM1 and 0.94 for MPI-ESM

360   during winter.

Table 2. Comparison between simulated areas of sea ice extents (in million km²) between the two models (CESM1 and MPI-ESM), for the Northern Hemisphere and around Greenland (see mask in Figure 1) for annual summer and winter extents, over the Common Era (1 – 2000 CE).

Sea ice extent (10^6 km²) during the Common Era		Northern Hemisphere			Greenland		
		Minimum extent	Annual average extent	Maximum extent	Minimum extent	Annual average extent	Maximum extent
CESM1	Summer	4.7	6.6	8.3	0.9	1.4	2.2
	Winter	15.0	16.2	17.6	4.1	4.6	5.2
MPI-ESM	Summer	3.6	5.2	7.0	0.4	0.8	1.3
	Winter	13.8	15.9	18.2	3.5	4.2	5.5

365
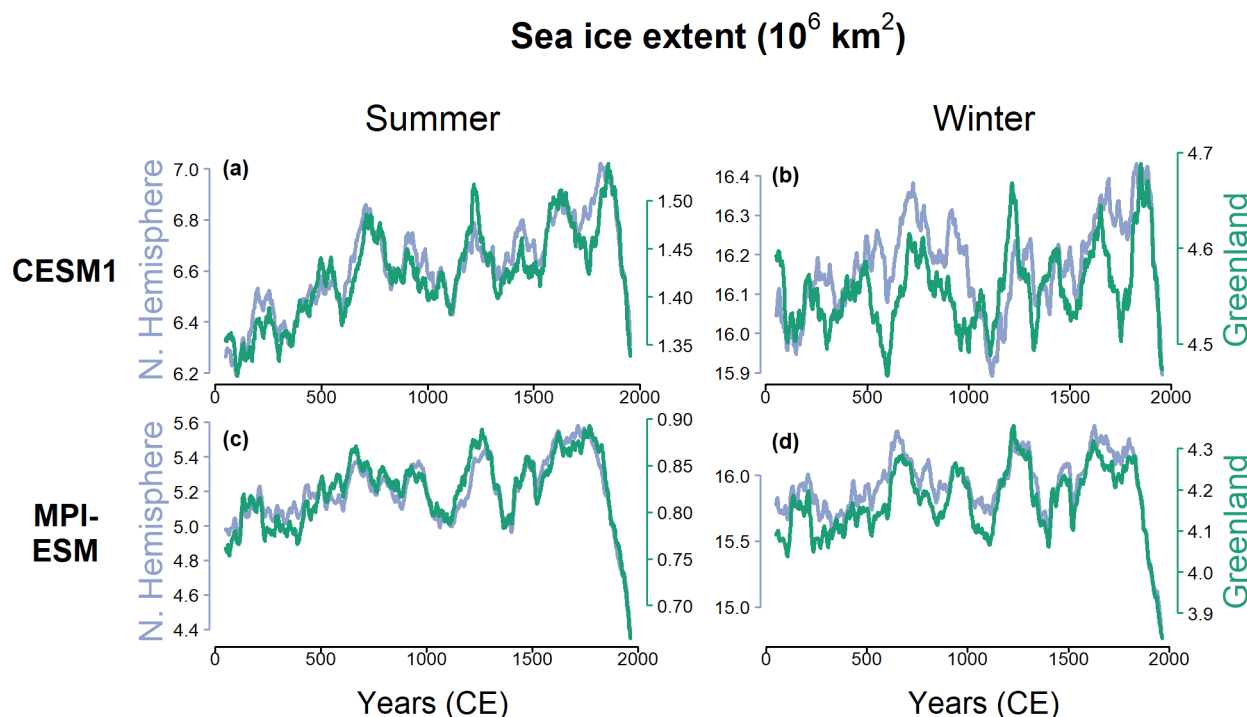
Sea ice extent (10^6 km^2)

Figure 5. Sea-ice extent (in million km^2; 100-year running mean) in both models, around Greenland (green) and in the whole Northern Hemisphere (blue), for boreal summer and winter seasons, over the Common Era. The very high agreement indicates that sea-ice proxy-compilations around Greenland are representative for the total northern hemispheric sea-ice extent on longer time scales.

A general positive trend of increasing sea ice is simulated until 1850 for both seasons, followed by a sharp decrease in the sea-ice area due to global warming (Table 3). During the pre-industrial period of the Common Era, sea-ice areas simulated for the whole Northern Hemisphere suggest expansion rates around 0.02 million km^2/100 years, and around 0.005 million km^2/100 years when simulated for the region around Greenland. Nevertheless, the expansion rates are so small that when the maximum extents were compared over the centuries before 1850, the maximum sea-ice cover expanded less than 1% per 100 years during the Common Era (Supp. Figure S5). After 1850, however, the trend shifted and both models registered decreases in sea-ice extent. In the whole Northern Hemisphere, the simulated sea-ice area shrunk around 0.7 million km^2/100 years (Table 3), corresponding to a loss ~ 9% area/100 years during summer and ~ 4% area/100 years during winter considering the maximum sea-ice extent during the Common Era. Around Greenland, simulations suggest sea-ice shrinkage of around 0.2 million km^2/100 years after 1850 (Table 3). When compared to the maximum sea-ice extent simulated for the Common Era, it represents a decrease of ~ 11% area /100 years in summer and ~ 6% of loss area /100 years in winter (Supp. Figure S5).

Table 3. Comparison between trends of simulated sea ice extent (in million km²/100 years) between the two models (CESM1 and MPI-ESM), in Northern Hemisphere and around Greenland (see mask in Figure 1), and for boreal summer and winter seasons, over the Common Era (1 – 2000 CE). The % values consider the maximum sea-ice extent simulated for the CE as reference.

Trend (10⁶ km² / 100 years)		Northern Hemisphere		Greenland	
		1 – 1850 CE	1851 – 2000 CE	1 – 1850 CE	1851 – 2000 CE
CESM1	summer	0.028	-0.762	0.006	-0.260
		(0.3%)	(-9.2%)	(0.3%)	(-11.9%)
	winter	0.009	-0.777	0.001	-0.328
		(0.1%)	(-4.4%)	(0.0%)	(-6.3%)
MPI-ESM	summer	0.021	-0.627	0.005	-0.138
		(0.3%)	(-8.9%)	(0.4%)	(-10.8%)
	winter	0.021	-0.692	0.008	-0.278
		(0.1%)	(-3.8%)	(0.2%)	(-5.1%)

390

To identify the main leading modes of sea-ice variability and their spatial loading patterns, we performed an EOF analysis for simulated sea-ice data after log-transforming the fractional data. Overall, the EOF analysis using both the 100-year running mean and the 100-years mean chunks data yield very similar spatial and temporal patterns in the first mode of variability (EOF 1 and PC1; Supp. Figures S6 and S7). This similarity shows that the approach of creating 100-years mean chunks for the proxy data will retrieve the main temporal behaviour and likely does not create artificial patterns in the EOF analysis. As the sea-ice proxies are mainly related to the period of sea-ice melt, we will focus the discussion on summer sea ice, i.e., minimum annual extent. Figure 6 shows the first and second mode of variability of summer sea ice. While the principal components' plots (PC1 and PC2) present the results from both 100-year running mean and 100-years mean chunks data, the EOF1 and EOF2 plots only present the 100-year running mean results.

400
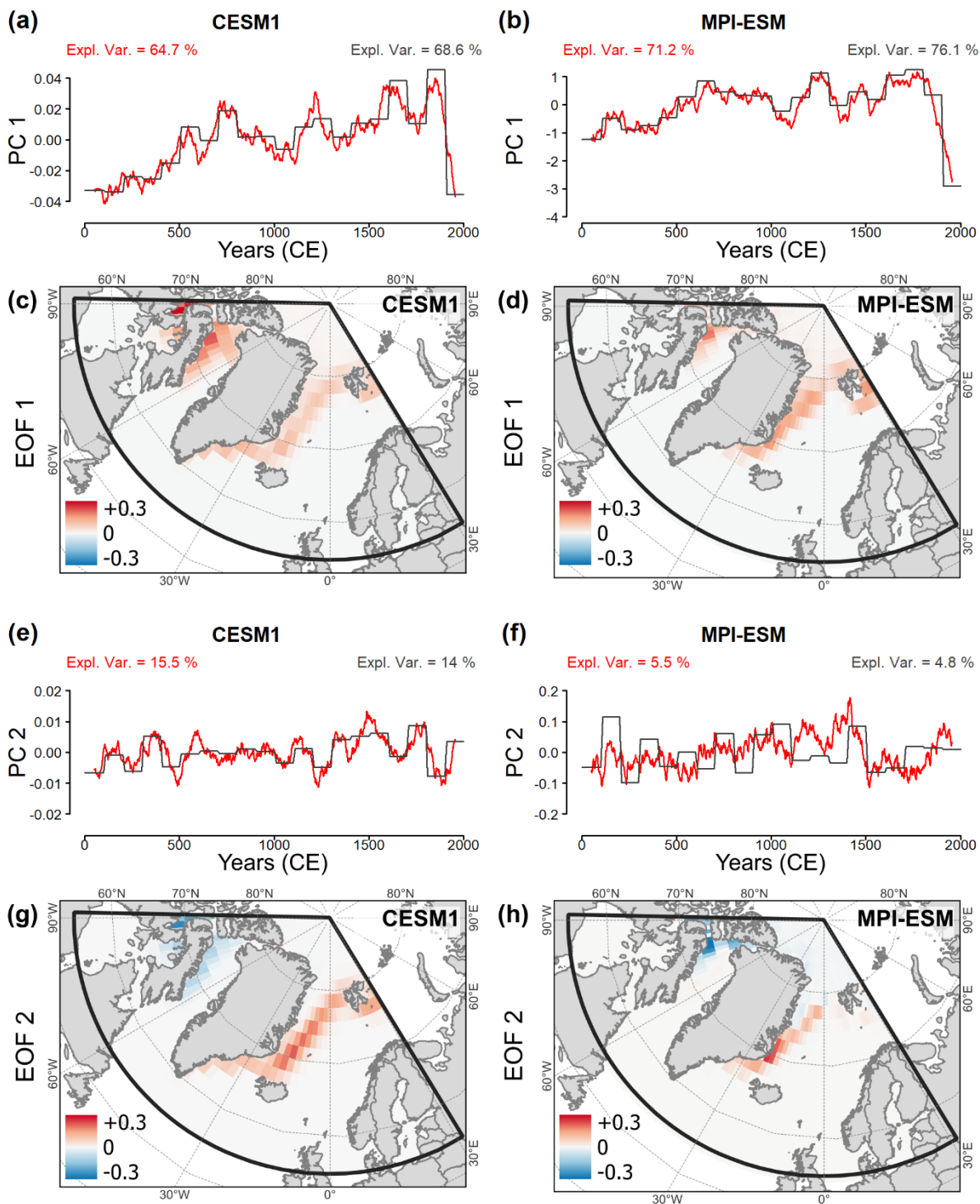
Figure 6. Results of empirical orthogonal function (EOF) analysis of the log-transformed sea ice fraction based on CESM1 (a,c,e,g) and MPI-ESM (b,df,h) data. Normalized principal components plots considering the 100-year running mean data (in red) and 100-years mean chunks mimicking proxy data resolution (in dark grey); PC1: (a) and (b); PC2: (e) and (f). First and second EOF mode loadings plots consider the 100-year running mean data; EOF1: (c) and (d); EOF2: (g) and (h).

PC1 from both models (CESM1 and MPI-ESM) show the expected long-term trend of increasing summer sea ice until around 1850 as in Figures 5a and 5c, followed by a sharp decrease (Figures 6a and b). The first leading mode explains more than 65% of the variability in the CESM1 model and more than 70% of variability in the MPI-ESM model. Spatially, most of the variance on multidecadal to centennial scale is concentrated in the Canadian channels and close to Greenland east coastline in both models (Figures 6c and d). PC2, on the other hand, displays a temporal pattern governed by internal variability and explains only around 15% and 5% of the variability in CESM1 and MPI-ESM models, respectively (Figures 6e and f). Although the temporal trends (PC2) were not quite similar between both models, the spatial distribution of EOF2 presented the same opposite pattern between Baffin Bay and Greenland Sea in both models (Figures 6g and h). This internal or residual variability might be related to changes in the sea-ice export through the Fram Strait, which affects the sea-ice fraction that reaches the Greenland Sea. Given the low explained variance in the simulations, we would not expect a large explanatory value in the noisier sea-ice proxy data. Thus, the first leading mode appears to contain most of the interpretable variance on larger than centennial scales over the last two millennia for the chosen area.

In addition to the increasing summer sea-ice trend prior to 1850, PC1 in both models contains some cyclicity. This was also present in PC2. A wavelet analysis of the annual summer sea-ice extent identified the main periodicities (Figure 7). For CESM1, the multidecadal cyclicity is centred around 21 and 33 years, and for MPI-ESM around 27, 41 and 74 years.
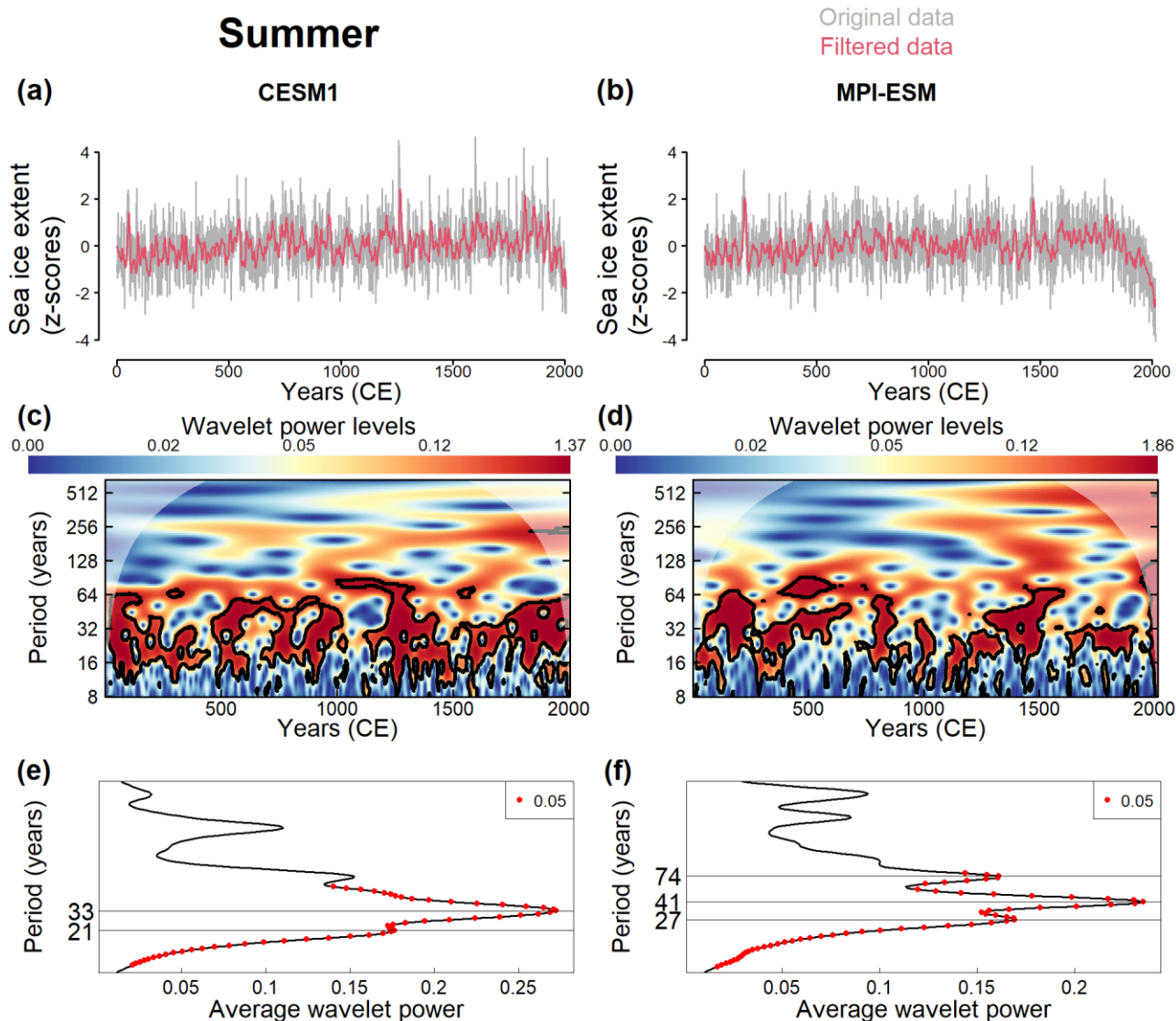
Figure 7. Wavelet analysis from both numerical models (CESM1 and MPI-ESM), considering summer sea ice extent. (a,b) Normalized time series of sea ice extent considering the original data (in grey) and the filtered data (in red). (c,d) Wavelet power spectrum and (e,f) global wavelet of the normalized signal on the time-frequency domain. Marked regions on the wavelet spectrum indicate significant power to a 95% confidence interval. The areas under the cone of influence show where edge effects are important.

One possible explanation for this multidecadal variability could be related to solar cycles. Solar activity has been reconstructed from measured concentrations of ^{14}C in tree rings and ^{10}Be in the GRIP ice core (Usoskin et al., 2006; Vonmoos et al., 2006) and other sources that are also used in the forcing of past2k simulations used here (Jungclaus et al., 2017). During the last 2000 years, one of the most pronounced periodicities is centred around ~80-year Gleissberg cycle

(Ma, 2009). During periods of high solar activity, summer sea ice might have presented smaller areas probably due to
435 enhanced melting. However, another possible explanation for the multidecadal cycles might be related to the Atlantic
Multidecadal Oscillation (AMO; Schlesinger and Ramankutty, 1994). The North Atlantic sea-surface temperature exhibits a
multi-decadal variability that cannot be fully explained by the radiative forcing (Ting et al., 2014) and is probably related to
the atmospheric-oceanic teleconnections affecting the heat transport in the North Atlantic (Fang et al., 2022). Positive phases
of AMO have been linked to a greater penetration of warm subtropical waters into the subpolar gyre (Buckley and Marshall,
440 2016), causing sea-ice retreat especially in the Atlantic sector of Arctic Ocean (Miles et al., 2016; Kumar et al., 2021).

3.3 Long-term trend vs short-term fluctuations

One of the aims of this study was to assess how well individual sea-ice proxy records are suited to reconstruct long-term sea-
ice trends and possibly multidecadal to centennial-scale variations that can be compared with climate model simulations.
Based on the proxy-based reconstruction compilation, it is evident that when clustered together, the common trend in proxy
445 records agrees well with the simulated summer sea-ice evolution. Both the reconstructions based on marine proxy data and
on numerical models demonstrate a long-term increase in sea-ice cover until around 1850, followed by a decrease in the
modern industrial period. This same behaviour was observed by Brennan and Hakim (2022). This increasing trend largely
agrees with recent temperature reconstructions compilations (McKay and Kaufman, 2014; PAGES 2k Consortium et al.,
2019), which observed a cooler period between 15th and 18th centuries followed by a sharp warming especially during the
450 20th century. However, there is discrepancy in the point of time when the long-term sea-ice trend changes. A sea-ice retreat is
apparent in the proxy records immediately following the LIA (from the 18th century; Figures 2a and 3c), while in the model
reconstructions this retreat begins clearly only in the 20th century (Figures 5a, 5c, 6a and 6b).

Interestingly, although individual proxy records presented some internal variability, they did not coincide with the
multidecadal-scale fluctuations observed in the numerical model reconstructions. In the records that presented significant (p
455 < 0.05) average wavelet power, the variability was mostly concentrated in periods around 30 and 50 years (Supp. Figures S8-
S14). This difference is likely caused by internal climate and ecosystem dynamics where proxy-based sea ice reconstructions
were affected by complex environmental parameters, while the physical models directly responded to large-scale
atmospheric forcing from variations in solar, volcanic, and orbital forcing. Furthermore, while the proxy records used here
have relatively high resolution (< 100 years), the resolution is generally not enough to capture multidecadal trends.
460 In addition to forced variability creating some co-variability between both simulations on multi-decadal to centennial
timescales (Figure 6), another explanation might be related to internal variability of the numerical models. The spatial
distribution of EOF2, associated with the multidecadal to centennial-scale fluctuations, in both models presented a similar
dipole pattern, with positive values observed in the Greenland Sea and negative values observed in the inner Baffin Bay.
However, their temporal patterns were not alike (Figures 6e and 6f). This inconsistency is probably caused by the low
465 explained variance of PC2 (15% for CESM1 and 5% for MPI-ESM), incorporating a large degree of residual noise.
Although the multidecadal and centennial variability of Arctic summer sea ice has been linked to changes in the northward

Atlantic and Pacific heat transport and in the Arctic dipole, there is still some significant variability between mean states of Arctic sea ice simulated by different models (Li et al., 2018).

Another explanation for the discrepancy observed in the multidecadal to centennial-scale fluctuations between proxy-based
470 and numerical model reconstructions might be related to seasonality. IP$_{25}$ is generally produced during the sympagic spring bloom prior to ice melt (Belt, 2019), while *I. minutum* cyst production probably occurs in the water column over the open water season (Heikkilä et al., 2016; Luostarinen et al., 2023). Thus, sea-ice proxies do not register sea ice in similar manner, although the all proxy-based sea-ice reconstructions resembled more the model-based summer season (annual minimum sea-ice extent) than the winter season (annual maximum sea-ice extent) simulations. Differences in the seasonal signal of sea ice
475 proxies can also cause inconsistent signals between paleorecords (Kolling et al., 2018). Early season sea-ice melt in absence of adequate light can cause a decrease in sympagic algal (IP$_{25}$) production. The cold freshwater layer from sea-ice melt in late spring and early summer, when light is not a limiting factor, might enhance the role of water-column diatom (*Fragilariopsis* spp., *Fossulaphycus arcticus*) and dinoflagellate (*Islandinium minutum*, *I.? cezare*) species used as sea-ice proxies.

480 Polynya formation can also add to the internal variability observed in the proxy-based reconstructions. Polynyas are areas of open water and thin ice in regions otherwise covered by sea ice and are common around Greenland (Smith Jr and Barber, 2007). In model simulations, however, much of the knowledge of the air–sea interaction over polynyas comes from atmospheric models, with not enough horizontal resolutions (often > 75 km) to properly resolve polynya dynamics (Moore and Våge, 2018). In turn, polynyas are often characterized as biological hot spots (Daase et al., 2020), with conspicuous sea-
485 ice proxy production (Limoges et al., 2020; Harning et al., 2023).

Lastly, marine terminating glaciers play an important role in coastal areas, creating possibly markedly differing sea-ice conditions and productivity when compared to sites further offshore (Kolling et al., 2018; Detlef et al., 2021; Jackson et al., 2021), adding to the internal variability of some proxy-based reconstructions. In these areas, glacier meltwater might generate a cold and brackish surface-water layer, causing salinity-driven stratification, an environment preferred by some sea
490 ice proxies, such as the diatoms *F. oceanica* and *F. reginae-jahniae* (Weckström et al., 2020).

Overall, the cluster analysis across a compilation of proxies presented here shows high potential to further analyse the presence of multi-decadal to multi-centennial variations in addition to long-term trends on longer timescales than the last 2000 years, depending on the core resolution. Apart from some potential local dependencies in proxy data described here, we consider it highly likely that significant (multi-)centennial variability could be detected in longer proxy records which might
495 improve the signal-to-noise-ratio in data. A recent assessment of over 120 records and several transient climate simulations has revealed a clear global presence of significant (multi-)centennial oscillation with 100–200 years periods during the Holocene with the strongest power in Arctic regions (Askjær et al., 2022).

4 Conclusions

In this study, our goal was to explore the long-term trends and low-frequency variability in proxy-based reconstructions and
500   to compare them with transient climate simulations. Both the clustered proxy-based sea-ice reconstructions and the model
simulations revealed a long-term increase in sea-ice cover over most of the Common Era. The maximum sea-ice cover was
recorded around the 17th and 18th centuries, identified as the Little Ice Age, probably related to intense volcanic activity. The
long-term sea-ice expansion over the Common Era has been largely explained by the decrease in the Northern Hemisphere
insolation due to orbital changes. The recent sea-ice retreat, on the other hand, was likely initiated by a recovery from the
505   volcanic dust emissions further amplified by anthropogenic greenhouse gas emissions towards the 20th century. Short-term
variability, however, was less coherent, whether among the proxy-based reconstructions, among the two numerical models,
or between the model simulations and the proxy reconstructions. Therefore, local-to-regional scale forcings, internal
variability and noise in the proxy data have a marked impact on short-them variability.

The good correspondence between clustered proxy-based records and numerical model reconstructions suggests that the
510   state-of-the-art sea-ice proxies are able to capture large-scale climate forcings. However, some of the individual sea-ice
proxy records incorporated local-scale environmental forcings that partially overrode large-scale forcings. Thus, considering
the ecology of the proxy matters: different proxy types represent different habitats and seasons, and incorporate noise from
environmental parameters other than sea ice, especially at coastal locations. Therefore, studying sea-ice history of a
particular region should ideally be based on several sea-ice proxy-based reconstructions. We suggest making use of stacked
515   sea-ice proxy records in future large-scale sea-ice studies, as they appear to show high agreement with transient climate
model simulations on longer timescales. Local reconstructions are equally important for reconstruction local-to-regional
scale patterns that are not captured by stacked records or climate models.

Code and data availability

Climate Data Operator software was used for analysing model data with CDO version 1.9.10 (Schulzweida, 2021;
520   https://code.mpimet.mpg.de/projects/cdo). The PMIP4 past2k simulations with MPI-ESM and CESM1 contribute to CMIP6
and can be retrieved via the Earth System Grid Federation network ESGF (e.g., https://esgf-data.dkrz.de/search/cmip6-dkrz/
or https://esgf.llnl.gov/, last access: 25 March 2022). The R environment was used to analyse the data using the packages
dplyr (https://cran.r-project.org/web/packages/dplyr/index.html), Hmisc (https://cran.r-
project.org/web/packages/Hmisc/index.html), ncdf4 (https://cran.r-project.org/web/packages/ncdf4/index.html), signal
525   (https://cran.r-project.org/web/packages/signal/index.html), TSclust (https://cran.r-
project.org/web/packages/TSclust/index.html), WaveletComp (https://cran.r-
project.org/web/packages/WaveletComp/index.html), and zoo (https://cran.r-project.org/web/packages/zoo/index.html).

Author contribution

Conceptualization: M.H., A.D. and F.S.; Funding acquisition: M.H., F.S.; Methodology and data analysis, A.D., F.S. and
530 K.P.; Writing – original draft preparation, A.D.; Writing – review and editing: A.D., K.P., F.S. and M.H.; Visualization: A.D; Project administration: M.H. All authors have read and agreed to the published version of the manuscript. A.D. is the corresponding author.

Acknowledgements

This study was funded by the Research Council of Finland (grants 296895, 328540 and 334509 to M.H.). F.S. received
535 funding from the Swedish Research Council for Sustainable Development (FORMAS 2020-01000). The Swedish-Finnish collaboration was funded by the Bolin Centre for Climate Research at Stockholm University and Arctic Avenue - a spearhead research project between the University of Helsinki and Stockholm University. The analysis of MPI-ESM and CESM1 simulations were enabled by resources provided by the National Academic Infrastructure for Supercomputing in Sweden (NAISS) at the National Supercomputer Centre (NSC), partially funded by the Swedish Research Council through
540 grant agreement no. 2022-06725. The model simulation with CESM1 was conducted with high-performance computing support from Yellowstone (ark:/85065/d7wd3xhc) provided by NCAR's Computational and Information Systems Laboratory, sponsored by the National Science Foundation.

References

Allan, E., de Vernal, A., Knudsen, M. F., Hillaire-Marcel, C., Moros, M., Ribeiro, S., Ouellet-Bernier, M. M., and
545 Seidenkrantz, M. S.: Late Holocene sea surface instabilities in the Disko Bugt area, West Greenland, in phase with δ18O oscillations at Camp Century, Paleoceanogr. Paleoclimatology, 33, 227–243, https://doi.org/10.1002/2017PA003289, 2018.

Andresen, C. S., McCarthy, D. J., Dylmer, C. V., Seidenkrantz, M. S., Kuijpers, A., and Lloyd, J. M.: Interaction between subsurface ocean waters and calving of the Jakobshavn Isbræ during the late Holocene, Holocene, 21, 211–224, https://doi.org/10.1177/0959683610378877, 2011.

550 Andrews, J. T., Belt, S. T., Olafsdottir, S., Massé, G., and Vare, L. L.: Sea ice and marine climate variability for NW Iceland/Denmark Strait over the last 2000 cal. yr BP, Holocene, 19, 775–784, https://doi.org/10.1177/0959683609105302, 2009.

Arrigo, K. R.: Sea ice ecosystems, Ann. Rev. Mar. Sci., 6, 439–467, https://doi.org/10.1146/annurev-marine-010213-135103, 2014.

555 Askjær, T. G., Zhang, Q., Schenk, F., Ljungqvist, F. C., Lu, Z., Brierley, C. M., Hopcroft, P. O., Jungclaus, J., Shi, X., Lohmann, G., Sun, W., Liu, J., Braconnot, P., Otto-Bliesner, B. L., Wu, Z., Yin, Q., Kang, Y., and Yang, H.: Multi-

centennial Holocene climate variability in proxy records and transient model simulations, Quat. Sci. Rev., 296, 107801, https://doi.org/10.1016/j.quascirev.2022.107801, 2022.

Bader, J., Jungclaus, J. H., Krivova, N., Lorenz, S., Maycock, A., Raddatz, T., Schmidt, H., Toohey, M., Wu, C. J., and
560   Claussen, M.: Global temperature modes shed light on the Holocene temperature conundrum, Nat. Commun., 11, 1–8, https://doi.org/10.1038/s41467-020-18478-6, 2020.

Belt, S. T.: Source-specific biomarkers as proxies for Arctic and Antarctic sea ice, Org. Geochem., 125, 277–298, https://doi.org/10.1016/j.orggeochem.2018.10.002, 2018.

Belt, S. T.: What do IP25 and related biomarkers really reveal about sea ice change?, Quat. Sci. Rev., 204, 216–219,
565   https://doi.org/10.1016/j.quascirev.2018.11.025, 2019.

Belt, S. T. and Müller, J.: The Arctic sea ice biomarker IP25: A review of current understanding, recommendations for future research and applications in palaeo sea ice reconstructions, Quat. Sci. Rev., 79, 9–25, https://doi.org/10.1016/j.quascirev.2012.12.001, 2013.

Belt, S. T., Vare, L. L., Massé, G., Manners, H. R., Price, J. C., MacLachlan, S. E., Andrews, J. T., and Schmidt, S.: Striking
570   similarities in temporal changes to spring sea ice occurrence across the central Canadian Arctic Archipelago over the last 7000 years, Quat. Sci. Rev., 29, 3489–3504, https://doi.org/10.1016/j.quascirev.2010.06.041, 2010.

Berger, A. L.: Long-Term variations of caloric insolation resulting from the Earth's orbital elements, Quat. Res., 9, 139–167, https://doi.org/10.1016/0033-5894(78)90064-9, 1978.

Berger, A. L. and Loutre, M. F.: Insolation values for the climate of the last 10 million years, Quat. Sci. Rev., 10, 297–317,
575   https://doi.org/10.1016/0277-3791(91)90033-Q, 1991.

Bintanja, R.: The impact of Arctic warming on increased rainfall, Sci. Rep., 8, 6–11, https://doi.org/10.1038/s41598-018-34450-3, 2018.

Brennan, M. K. and Hakim, G. J.: Reconstructing Arctic sea ice over the Common Era using data assimilation, J. Clim., 35, 1231–1247, https://doi.org/10.1175/JCLI-D-21-0099.1, 2022.

580   Brovkin, V., Lorenz, S., Raddatz, T., Ilyina, T., Stemmler, I., Toohey, M., and Claussen, M.: What was the source of the atmospheric CO2 increase during the Holocene?, Biogeosciences, 16, 2543–2555, https://doi.org/10.5194/bg-16-2543-2019, 2019.

Brown, T. A., Rad-Menéndez, C., Ray, J. L., Skaar, K. S., Thomas, N., Ruiz-Gonzalez, C., and Leu, E.: Influence of nutrient availability on Arctic sea ice diatom HBI lipid synthesis, Org. Geochem., 141, 103977,
585   https://doi.org/10.1016/j.orggeochem.2020.103977, 2020.

Buckley, M. W. and Marshall, J.: Observations, inferences, and mechanisms of the Atlantic Meridional Overturning Circulation: A review, Rev. Geophys., 54, 5–63, https://doi.org/10.1002/2015RG000493, 2016.

Büntgen, U., Arseneault, D., Boucher, É., Churakova (Sidorova), O. V., Gennaretti, F., Crivellaro, A., Hughes, M. K., Kirdyanov, A. V., Klippel, L., Krusic, P. J., Linderholm, H. W., Ljungqvist, F. C., Ludescher, J., McCormick, M., Myglan,
590   V. S., Nicolussi, K., Piermattei, A., Oppenheimer, C., Reinig, F., Sigl, M., Vaganov, E. A., and Esper, J.: Prominent role of

volcanism in Common Era climate variability and human history, Dendrochronologia, 64, https://doi.org/10.1016/j.dendro.2020.125757, 2020.

Cabedo-Sanz, P. and Belt, S. T.: Seasonal sea ice variability in eastern Fram Strait over the last 2000 years, Arktos, 2, 1–12, https://doi.org/10.1007/s41063-016-0023-2, 2016.

595 Cabedo-Sanz, P., Belt, S. T., Jennings, A. E., Andrews, J. T., and Geirsdóttir, Á.: Variability in drift ice export from the Arctic Ocean to the North Icelandic Shelf over the last 8000 years: A multi-proxy evaluation, Quat. Sci. Rev., 146, 99–115, https://doi.org/10.1016/j.quascirev.2016.06.012, 2016.

Craig, A. P., Vertenstein, M., and Jacob, R.: A new flexible coupler for earth system modeling developed for CCSM4 and CESM1, Int. J. High Perform. Comput. Appl., 26, 31–42, https://doi.org/10.1177/1094342011428141, 2012.

600 Daase, M., Berge, J., Søreide, J. E., and Falk-Petersen, S.: Ecology of Arctic pelagic communities, in: Arctic Ecology, edited by: Thomas, D. N., John Wiley & Sons Ltd, 219–260, 2020.

Dai, A., Luo, D., Song, M., and Liu, J.: Arctic amplification is caused by sea-ice loss under increasing CO_2, Nat. Commun., 10, 1–13, https://doi.org/10.1038/s41467-018-07954-9, 2019.

Detlef, H., Reilly, B., Jennings, A., Mørk Jensen, M., O'Regan, M., Glasius, M., Olsen, J., Jakobsson, M., and Pearce, C.:
605 Holocene sea-ice dynamics in Petermann Fjord in relation to ice tongue stability and Nares Strait ice arch formation, Cryosphere, 15, 4357–4380, https://doi.org/10.5194/tc-15-4357-2021, 2021.

van Dijk, E., Jungclaus, J., Lorenz, S., Timmreck, C., and Krüger, K.: Was there a volcanic-induced long-lasting cooling over the Northern Hemisphere in the mid-6th-7th century?, Clim. Past, 18, 1601–1623, https://doi.org/10.5194/cp-18-1601-2022, 2022.

610 Eamer, J., Donaldson, G. M., Gaston, A. J., Kosobokova, K. N., Lárusson, K. F., Melnikov, I. A., Reist, J. D., Richardson, E., Staples, L., and von Quillfeldt, C. H.: Life Linked to Ice: A guide to sea-ice-associated biodiversity in this time of rapid change, CAFF Assessment Series No. 10. Conservation of Arctic Flora and Fauna, Iceland, 01–153 pp., 2013.

Fang, M., Li, X., Chen, H. W., and Chen, D.: Arctic amplification modulated by Atlantic Multidecadal Oscillation and greenhouse forcing on multidecadal to century scales, Nat. Commun., 13, 1–8, https://doi.org/10.1038/s41467-022-29523-x,
615 2022.

Fox-Kemper, B., Hewitt, H. T., Xiao, C., Aðalgeirsdóttir, G., Drijfhout, S. S., Edwards, T. L., Golledge, N. R., Hemer, M., Kopp, R. E., Krinner, G., Mix, A. C., Notz, D., Nowicki, S., Nurhati, I. S., Ruiz, L., Sallée, J.-B., Slangen, A. B. A., and Yu, Y.: Ocean, cryosphere and sea level change, in: Climate Change 2021: The Physical Science Basis. Contribution of Working Group I to the Sixth Assessment Report of the Intergovernmental Panel on Climate Change, edited by: Masson-Delmotte,
620 V., Zhai, P., Pirani, A., Connors, S. L., Péan, C., Berger, S., Caud, N., Chen, Y., Goldfarb, L., Gomis, M. I., Huang, M., Leitzell, K., Lonnoy, E., Matthews, J. B. R., Maycock, T. K., Waterfield, T., Yelekçi, O., Yu, R., and Zhou, B., Cambridge University Press, Cambridge, United Kingdom and New York, NY, USA, 1211–1362, https://doi.org/10.1017/9781009157896.011, 2021.

Goosse, H., Roche, D. M., Mairesse, A., and Berger, M.: Modelling past sea ice changes, Quat. Sci. Rev., 79, 191–206,
625   https://doi.org/10.1016/j.quascirev.2013.03.011, 2013.

Goosse, H., Kay, J. E., Armour, K. C., Bodas-Salcedo, A., Chepfer, H., Docquier, D., Jonko, A., Kushner, P. J., Lecomte, O.,
Massonnet, F., Park, H. S., Pithan, F., Svensson, G., and Vancoppenolle, M.: Quantifying climate feedbacks in polar regions,
Nat. Commun., 9, https://doi.org/10.1038/s41467-018-04173-0, 2018.

Harning, D. J., Holman, B., Woelders, L., Jennings, A. E., and Sepúlveda, J.: Biomarker characterization of the North Water
630   Polynya, Baffin Bay: implications for local sea ice and temperature proxies, Biogeosciences, 20, 229–249,
https://doi.org/10.5194/bg-20-229-2023, 2023.

Harrell   Jr.,   F.   E.:   Hmisc: Harrell   Miscellaneous.   R   package   version   4.7-0,   https://cran.r-
project.org/web/packages/Hmisc/index.html, 2022.

Head, M. J., Harland, R., and Matthiessen, J.: Cold marine indicators of the late Quaternary: the new dinoflagellate cyst
635   genus Islandinium and related morphotypes, J. Quat. Sci., 16, 621–636, https://doi.org/10.1002/jqs.657, 2001.

Heikkilä, M., Pospelova, V., Forest, A., Stern, G. A., Fortier, L., and Macdonald, R. W.: Dinoflagellate cyst production over
an   annual   cycle   in   seasonally   ice-covered   Hudson   Bay,   Mar.   Micropaleontol.,   125,   1–24,
https://doi.org/10.1016/j.marmicro.2016.02.005, 2016.

Heikkilä, M., Ribeiro, S., Weckström, K., and Pieńkowski, A. J.: Predicting the future of coastal marine ecosystems in the
640   rapidly   changing   Arctic: The   potential   of   palaeoenvironmental   records,   Anthropocene,   37,   100319,
https://doi.org/10.1016/j.ancene.2021.100319, 2022.

Hop, H. and Gjøsæter, H.: Polar cod (Boreogadus saida) and capelin (Mallotus villosus) as key species in marine food webs
of the Arctic and the Barents Sea, Mar. Biol. Res., 9, 878–894, https://doi.org/10.1080/17451000.2013.775458, 2013.

Hurtt, G. C., Chini, L. P., Frolking, S., Betts, R. A., Feddema, J., Fischer, G., Fisk, J. P., Hibbard, K., Houghton, R. A.,
645   Janetos, A., Jones, C. D., Kindermann, G., Kinoshita, T., Klein Goldewijk, K., Riahi, K., Shevliakova, E., Smith, S.,
Stehfest, E., Thomson, A., Thornton, P., van Vuuren, D. P., and Wang, Y. P.: Harmonization of land-use scenarios for the
period 1500-2100: 600 years of global gridded annual land-use transitions, wood harvest, and resulting secondary lands,
Clim. Change, 109, 117–161, https://doi.org/10.1007/s10584-011-0153-2, 2011.

IPCC: Summary for policymakers, in: Climate Change 2021: The Physical Science Basis. Contribution of Working Group I
650   to the Sixth Assessment Report of the Intergovernmental Panel on Climate Change, edited by: Masson-Delmotte, V., Zhai,
P., Pirani, A., Connors, S. L., Péan, C., Berger, S., Caud, N., Chen, Y., Goldfarb, L., Gomis, M. I., Huang, M., Leitzell, K.,
Lonnoy, E., Matthews, J. B. R., Maycock, T. K., Waterfield, T., Yelekçi, O., Yu, R., and Zhou, B., Cambridge University
Press, 3–32, https://doi.org/10.1017/9781009157896.001, 2021.

Jackson, R., Kvorning, A. B., Limoges, A., Georgiadis, E., Olsen, S. M., Tallberg, P., Andersen, T. J., Mikkelsen, N.,
655   Giraudeau, J., Massé, G., Wacker, L., and Ribeiro, S.: Holocene polynya dynamics and their interaction with oceanic heat
transport in northernmost Baffin Bay, Sci. Rep., 11, https://doi.org/10.1038/s41598-021-88517-9, 2021.

Jungclaus, J. H., Bard, E., Baroni, M., Braconnot, P., Cao, J., Chini, L. P., Egorova, T., Evans, M., Fidel González-Rouco, J., Goosse, H., Hurtt, G. C., Joos, F., Kaplan, J. O., Khodri, M., Klein Goldewijk, K., Krivova, N., Legrande, A. N., Lorenz, S. J., Luterbacher, J., Man, W., Maycock, A. C., Meinshausen, M., Moberg, A., Muscheler, R., Nehrbass-Ahles, C., Otto-

660   Bliesner, B. I., Phipps, S. J., Pongratz, J., Rozanov, E., Schmidt, G. A., Schmidt, H., Schmutz, W., Schurer, A., Shapiro, A. I., Sigl, M., Smerdon, J. E., Solanki, S. K., Timmreck, C., Toohey, M., Usoskin, I. G., Wagner, S., Wu, C. J., Leng Yeo, K., Zanchettin, D., Zhang, Q., and Zorita, E.: The PMIP4 contribution to CMIP6 - Part 3: The last millennium, scientific objective, and experimental design for the PMIP4 past1000 simulations, Geosci. Model Dev., 10, 4005–4033, https://doi.org/10.5194/gmd-10-4005-2017, 2017.

665   Kinnard, C., Zdanowicz, C. M., Fisher, D. A., Isaksson, E., de Vernal, A., and Thompson, L. G.: Reconstructed changes in Arctic sea ice over the past 1,450 years, Nature, 479, 509–512, https://doi.org/10.1038/nature10581, 2011.

Kirchner, N., Kuttenkeuler, J., Rosqvist, G., Hancke, M., Weckström, J., Weckström, K., Schenk, F., Eriksson, P., Kirchner, N., Kuttenkeuler, J., Rosqvist, G., and Hancke, M.: A first continuous three-year temperature record from the dimictic arctic – alpine Lake Tarfala , northern Sweden, Arctic, Antarct. Alp. Res., 53, 69–79,

670   https://doi.org/10.1080/15230430.2021.1886577, 2021.

Klein Goldewijk, K., Beusen, A., and Janssen, P.: Long-term dynamic modeling of global population and built-up area in a spatially explicit way: HYDE 3.1, Holocene, 20, 565–573, https://doi.org/10.1177/0959683609356587, 2010.

Kolling, H. M., Stein, R., Fahl, K., Perner, K., and Moros, M.: Short-term variability in late Holocene sea ice cover on the East Greenland Shelf and its driving mechanisms, Palaeogeogr. Palaeoclimatol. Palaeoecol., 485, 336–350,

675   https://doi.org/10.1016/j.palaeo.2017.06.024, 2017.

Kolling, H. M., Stein, R., Fahl, K., Perner, K., and Moros, M.: New insights into sea ice changes over the past 2.2 kyr in Disko Bugt, West Greenland, Arktos, 4, 1–20, https://doi.org/10.1007/s41063-018-0045-z, 2018.

Köseoğlu, D., Belt, S. T., Husum, K., and Knies, J.: An assessment of biomarker-based multivariate classification methods versus the PIP25 index for paleo Arctic sea ice reconstruction, Org. Geochem., 125, 82–94,

680   https://doi.org/10.1016/j.orggeochem.2018.08.014, 2018.

Kretschmer, M., Zappa, G., and Shepherd, T. G.: The role of Barents–Kara sea ice loss in projected polar vortex changes, Weather Clim. Dyn., 1, 715–730, https://doi.org/10.5194/wcd-1-715-2020, 2020.

Krivova, N. A., Solanki, S. K., and Unruh, Y. C.: Towards a long-term record of solar total and spectral irradiance, J. Atmos. Solar-Terrestrial Phys., 73, 223–234, https://doi.org/10.1016/j.jastp.2009.11.013, 2011.

685   Kumar, A., Yadav, J., and Mohan, R.: Spatio-temporal change and variability of Barents-Kara sea ice, in the Arctic: Ocean and atmospheric implications, Sci. Total Environ., 753, 142046, https://doi.org/10.1016/j.scitotenv.2020.142046, 2021.

Lannuzel, D., Tedesco, L., van Leeuwe, M., Campbell, K., Flores, H., Delille, B., Miller, L., Stefels, J., Assmy, P., Bowman, J., Brown, K., Castellani, G., Chierici, M., Crabeck, O., Damm, E., Else, B., Fransson, A., Fripiat, F., Geilfus, N. X., Jacques, C., Jones, E., Kaartokallio, H., Kotovitch, M., Meiners, K., Moreau, S., Nomura, D., Peeken, I., Rintala, J. M.,

690   Steiner, N., Tison, J. L., Vancoppenolle, M., Van der Linden, F., Vichi, M., and Wongpan, P.: The future of Arctic sea-ice

biogeochemistry and ice-associated ecosystems, Nat. Clim. Chang., 10, 983–992, https://doi.org/10.1038/s41558-020-00940-4, 2020.

Li, D., Zhang, R., and Knutson, T.: Comparison of mechanisms for low-frequency variability of summer Arctic sea ice in three coupled models, J. Clim., 31, 1205–1226, https://doi.org/10.1175/JCLI-D-16-0617.1, 2018.

695 Ligges, U., Short, T., Kienzle, P., Schnackenberg, S., Billinghurst, D., Borchers, H.-W., Carezia, A., Dupuis, P., Eaton, J. W., Farhi, E., Habel, K., Hornik, K., Krey, S., Lash, B., Leisch, F., Mersmann, O., Neis, P., Ruohio, J., III, J. O. S., Stewart, D., and Weingessel, A.: signal: Signal processing. R package version 0.7-7, https://cran.r-project.org/web/packages/signal/index.html, 2022.

Limoges, A., Massé, G., Weckström, K., Poulin, M., Ellegaard, M., Heikkilä, M., Geilfus, N.-X., Sejr, M. K., Rysgaard, S.,
700 and Ribeiro, S.: Spring succession and vertical export of diatoms and IP25 in a seasonally ice-covered high Arctic fjord, Front. Earth Sci., 6, 1–15, https://doi.org/10.3389/feart.2018.00226, 2018.

Limoges, A., Weckström, K., Ribeiro, S., Georgiadis, E., Hansen, K. E., Martinez, P., Seidenkrantz, M. S., Giraudeau, J., Crosta, X., and Massé, G.: Learning from the past: Impact of the Arctic Oscillation on sea ice and marine productivity off northwest Greenland over the last 9,000 years, Glob. Chang. Biol., 26, 6767–6786, https://doi.org/10.1111/gcb.15334, 2020.

705 Lin, J., Keogh, E., Wei, L., and Lonardi, S.: Experiencing SAX: A novel symbolic representation of time series, Data Min. Knowl. Discov., 15, 107–144, https://doi.org/10.1007/s10618-007-0064-z, 2007.

Luostarinen, T., Ribeiro, S., Weckström, K., Sejr, M., Meire, L., Tallberg, P., and Heikkilä, M.: An annual cycle of diatom succession in two contrasting Greenlandic fjords: from simple sea-ice indicators to varied seasonal strategists, Mar. Micropaleontol., 158, 101873, https://doi.org/10.1016/j.marmicro.2020.101873, 2020.

710 Luostarinen, T., Weckström, K., Ehn, J., Kamula, M., Burson, A., Diaz, A., Massé, G., Mcgowan, S., Kuzyk, Z. Z., and Heikkilä, M.: Seasonal and habitat-based variations in vertical export of biogenic sea-ice proxies in Hudson Bay, Commun. Earth Environ., 4, 1–13, https://doi.org/10.1038/s43247-023-00719-3, 2023.

Ma, L. H.: Gleissberg cycle of solar activity over the last 7000 years, New Astron., 14, 1–3, https://doi.org/10.1016/j.newast.2008.04.001, 2009.

715 MacFarling Meure, C., Etheridge, D., Trudinger, C., Steele, P., Langenfelds, R., Van Ommen, T., Smith, A., and Elkins, J.: Law Dome CO2, CH4 and N2O ice core records extended to 2000 years BP, Geophys. Res. Lett., 33, 2000–2003, https://doi.org/10.1029/2006GL026152, 2006.

Macias-Fauria, M. and Post, E.: Effects of sea ice on Arctic biota: an emerging crisis discipline, Biol. Lett., 14, 20170702, https://doi.org/10.1098/rsbl.2018.0265, 2018.

720 Maffezzoli, N., Risebrobakken, B., Miles, M. W., Vallelonga, P., Berben, S. M. P., Scoto, F., Edwards, R., Kjær, H. A., Sadatzki, H., Saiz-Lopez, A., Turetta, C., Barbante, C., Vinther, B., and Spolaor, A.: Sea ice in the northern North Atlantic through the Holocene: Evidence from ice cores and marine sediment records, Quat. Sci. Rev., 273, https://doi.org/10.1016/j.quascirev.2021.107249, 2021.

Marret, F., Bradley, L., de Vernal, A., Hardy, W., Kim, S. Y., Mudie, P., Penaud, A., Pospelova, V., Price, A. M., Radi, T.,
725 and Rochon, A.: From bi-polar to regional distribution of modern dinoflagellate cysts, an overview of their biogeography,
    Mar. Micropaleontol., 159, 101753, https://doi.org/10.1016/j.marmicro.2019.101753, 2020.

Mauritsen, T., Bader, J., Becker, T., Behrens, J., Bittner, M., Brokopf, R., Brovkin, V., Claussen, M., Crueger, T., Esch, M.,
    Fast, I., Fiedler, S., Fläschner, D., Gayler, V., Giorgetta, M., Goll, D. S., Haak, H., Hagemann, S., Hedemann, C.,
    Hohenegger, C., Ilyina, T., Jahns, T., Jimenéz-de-la-Cuesta, D., Jungclaus, J., Kleinen, T., Kloster, S., Kracher, D., Kinne,
730 S., Kleberg, D., Lasslop, G., Kornblueh, L., Marotzke, J., Matei, D., Meraner, K., Mikolajewicz, U., Modali, K., Möbis, B.,
    Müller, W. A., Nabel, J. E. M. S., Nam, C. C. W., Notz, D., Nyawira, S. S., Paulsen, H., Peters, K., Pincus, R., Pohlmann,
    H., Pongratz, J., Popp, M., Raddatz, T. J., Rast, S., Redler, R., Reick, C. H., Rohrschneider, T., Schemann, V., Schmidt, H.,
    Schnur, R., Schulzweida, U., Six, K. D., Stein, L., Stemmler, I., Stevens, B., von Storch, J. S., Tian, F., Voigt, A., Vrese, P.,
    Wieners, K. H., Wilkenskjeld, S., Winkler, A., and Roeckner, E.: Developments in the MPI-M Earth System Model version
735 1.2 (MPI-ESM1.2) and its response to increasing CO_2, J. Adv. Model. Earth Syst., 11, 998–1038,
    https://doi.org/10.1029/2018MS001400, 2019.

McKay, N. P. and Kaufman, D. S.: An extended Arctic proxy temperature database for the past 2,000 years, Sci. Data, 1, 1–
    10, https://doi.org/10.1038/sdata.2014.26, 2014.

Miettinen, A., Divine, D., Kocx, N., Godtliebsen, F., and Hall, I. R.: Multicentennial variability of the sea surface
740 temperature gradient across the subpolar North Atlantic over the last 2.8 kyr, J. Clim., 25, 4205–4219,
    https://doi.org/10.1175/JCLI-D-11-00581.1, 2012.

Miles, M. W., Divine, D. V., Furevik, T., Jansen, E., Moros, M., and Ogilvie, A. E. J.: A signal of persistent Atlantic
    multidecadal variability in Arctic sea ice, Geophys. Res. Lett., 1–8, https://doi.org/10.1002/2013GL058084.Received, 2016.

Miles, M. W., Andresen, C. S., and Dylmer, C. V.: Evidence for extreme export of Arctic sea ice leading the abrupt onset of
745 the Little Ice Age, Sci. Adv., 6, https://doi.org/10.1126/sciadv.aba4320, 2020.

Moffa-Sánchez, P., Moreno-Chamarro, E., Reynolds, D. J., Ortega, P., Cunningham, L., Swingedouw, D., Amrhein, D. E.,
    Halfar, J., Jonkers, L., Jungclaus, J. H., Perner, K., Wanamaker, A., and Yeager, S.: Variability in the northern North
    Atlantic and Arctic oceans across the last two millennia: A review, Paleoceanogr. Paleoclimatology, 34, 1399–1436,
    https://doi.org/10.1029/2018PA003508, 2019.

750 Montero, P. and Vilar, J. A.: TSclust: an R Package for time series clustering, J. Stat. Softw., 62, 1–43, 2014.

Moore, G. W. K. and Våge, K.: Impact of model resolution on the representation of the air–sea interaction associated with
    the North Water Polynya, Q. J. R. Meteorol. Soc., 144, 1474–1489, https://doi.org/10.1002/qj.3295, 2018.

Müller, J., Werner, K., Stein, R., Fahl, K., Moros, M., and Jansen, E.: Holocene cooling culminates in sea ice oscillations in
    Fram Strait, Quat. Sci. Rev., 47, 1–14, https://doi.org/10.1016/j.quascirev.2012.04.024, 2012.

755 Oksman, M., Juggins, S., Miettinen, A., Witkowski, A., and Weckström, K.: The biogeography and ecology of common
    diatom species in the northern North Atlantic, and their implications for paleoceanographic reconstructions, Mar.
    Micropaleontol., 148, 1–28, https://doi.org/10.1016/j.marmicro.2019.02.002, 2019.

PAGES 2k Consortium, Neukom, R., Barboza, L. A., Erb, M. P., Shi, F., Emile-Geay, J., Evans, M. N., Franke, J., Kaufman, D. S., Lücke, L., Rehfeld, K., Schurer, A., Zhu, F., Brönnimann, S., Hakim, G. J., Henley, B. J., Ljungqvist, F. C., McKay,

760 N. P., Valler, V., and von Gunten, L.: Consistent multidecadal variability in global temperature reconstructions and simulations over the Common Era, Nat. Geosci., 12, 643–649, https://doi.org/10.1038/s41561-019-0400-0, 2019.

Pierce, D.: ncdf4: Interface to unidata netCDF (version 4 or earlier) format data files. R package version 1.15, https://cran.r-project.org/web/packages/ncdf4/index.html, 2015.

QGIS Development Team: QGIS Geographic Information System. Open Source Geospatial Foundation Project. Version

765 3.26.2 Buenos Aires, 2022.

R Core Team: R: A language and environment for statistical computing, https://www.r-project.org/, 2022.

Rantanen, M., Karpechko, A. Y., Lipponen, A., Nordling, K., Hyvärinen, O., Ruosteenoja, K., Vihma, T., and Laaksonen, A.: The Arctic has warmed nearly four times faster than the globe since 1979, Commun. Earth Environ., 3, 1–10, https://doi.org/10.1038/s43247-022-00498-3, 2022.

770 Roesch, A. and Schmidbauer, H.: WaveletComp: Computational Wavelet Analysis. R package version 1.1, https://cran.r-project.org/package=WaveletComp, 2018.

Ryan, J. C., Smith, L. C., Cooley, S. W., Pearson, B., Wever, N., Keenan, E., and Lenaerts, J. T. M.: Decreasing surface albedo signifies a growing importance of clouds for Greenland Ice Sheet meltwater production, Nat. Commun., 13, 1–8, https://doi.org/10.1038/s41467-022-31434-w, 2022.

775 Schlesinger, M. E. and Ramankutty, N.: An oscillation in the global climate system of period 65-70 years, Lett. to Nat., 367, 723–726, 1994.

Schulzweida, U.: Climate Data Operator (CDO) User Guide. Version 2.0.5, https://doi.org/10.5281/zenodo.3539275, 2021.

Sha, L., Jiang, H., Seidenkrantz, M. S., Li, D., Andresen, C. S., Knudsen, K. L., Liu, Y., and Zhao, M.: A record of Holocene sea-ice variability off West Greenland and its potential forcing factors, Palaeogeogr. Palaeoclimatol. Palaeoecol., 475, 115–

780 124, https://doi.org/10.1016/j.palaeo.2017.03.022, 2017.

Shuman, B. N., Routson, C., McKay, N. P., Fritz, S., Kaufman, D. S., Kirby, M. E., Nolan, C., Pederson, G. T., and St-Jacques, J. M.: Placing the Common Era in a Holocene context: Millennial to centennial patterns and trends in the hydroclimate of North America over the past 2000 years, Clim. Past, 14, 665–686, https://doi.org/10.5194/cp-14-665-2018, 2018.

785 Smith Jr, W. O. and Barber, D. (Eds.): Polynyas: Windows to the World, Elsevier, 474 pp., 2007.

Sun, L., Alexander, M., and Deser, C.: Evolution of the global coupled climate response to Arctic sea ice loss during 1990-2090 and its contribution to climate change, J. Clim., 31, 7823–7843, https://doi.org/10.1175/JCLI-D-18-0134.1, 2018.

Syring, N., Stein, R., Fahl, K., Vahlenkamp, M., Zehnich, M., Spielhagen, R. F., and Niessen, F.: Holocene changes in sea-ice cover and polynya formation along the eastern North Greenland shelf: New insights from biomarker records, Quat. Sci.

790 Rev., 231, 106173, https://doi.org/10.1016/j.quascirev.2020.106173, 2020.

Talley, L. D., Pickard, G. L., Emery, W. J., and Swift, J. H.: Arctic Ocean and Nordic Seas, in: Descriptive Physical Oceanography: An Introduction, 401–436, https://doi.org/10.1016/b978-0-7506-4552-2.10012-5, 2011.

Ting, M., Kushnir, Y., and Li, C.: North Atlantic Multidecadal SST Oscillation: External forcing versus internal variability, J. Mar. Syst., 133, 27–38, https://doi.org/10.1016/j.jmarsys.2013.07.006, 2014.

795 Toohey, M., Stevens, B., Schmidt, H., and Timmreck, C.: Easy Volcanic Aerosol (EVA v1.0): An idealized forcing generator for climate simulations, Geosci. Model Dev., 9, 4049–4070, https://doi.org/10.5194/gmd-9-4049-2016, 2016.

Tsoy, I. B., Obrezkova, M. S., Aksentov, K. I., Kolesnik, A. N., and Panov, V. S.: Late Holocene environmental changes in the southwestern Chukchi Sea inferred from diatom analysis, Russ. J. Mar. Biol., 43, 276–285, https://doi.org/10.1134/S1063074017040113, 2017.

800 Usoskin, I. G., Solanki, S. K., and Korte, M.: Solar activity reconstructed over the last 7000 years: The influence of geomagnetic field changes, Geophys. Res. Lett., 33, 2–5, https://doi.org/10.1029/2006GL025921, 2006.

de Vernal, A. and Marret, F.: Organic-walled dinoflagellate cysts: tracers of sea-surface conditions, in: Proxies in Late Cenozoic Paleoceanography, vol. 1, edited by: Hillaire–Marcel, C. and Vernal, A. de, Elsevier, Amsterdam, 371–408, https://doi.org/10.1016/S1572-5480(07)01014-7, 2007.

805 de Vernal, A., Hillaire-Marcel, C., Rochon, A., Fréchette, B., Henry, M., Solignac, S., and Bonnet, S.: Dinocyst-based reconstructions of sea ice cover concentration during the Holocene in the Arctic Ocean, the northern North Atlantic Ocean and its adjacent seas, Quat. Sci. Rev., 79, 111–121, https://doi.org/10.1016/j.quascirev.2013.07.006, 2013.

de Vernal, A., Radi, T., Zaragosi, S., Van Nieuwenhove, N., Rochon, A., Allan, E., De Schepper, S., Eynaud, F., Head, M. J., Limoges, A., Londeix, L., Marret, F., Matthiessen, J., Penaud, A., Pospelova, V., Price, A., and Richerol, T.: Distribution 810 of common modern dinoflagellate cyst taxa in surface sediments of the Northern Hemisphere in relation to environmental parameters: The new n=1968 database, Mar. Micropaleontol., 159, 101796, https://doi.org/10.1016/j.marmicro.2019.101796, 2020.

Vonmoos, M., Beer, J., and Muscheler, R.: Large variations in Holocene solar activity: Constraints from 10Be in the Greenland Ice Core Project ice core, J. Geophys. Res. Sp. Phys., 111, 1–14, https://doi.org/10.1029/2005JA011500, 2006.

815 Wang, J., Yang, B., Fang, M., Wang, Z., Liu, J., and Kang, S.: Synchronization of summer peak temperatures in the Medieval Climate Anomaly and Little Ice Age across the Northern Hemisphere varies with space and time scales, Clim. Dyn., 1–16, https://doi.org/10.1007/s00382-022-06524-6, 2022.

Wanner, H., Solomina, O., Grosjean, M., Ritz, S. P., and Jetel, M.: Structure and origin of Holocene cold events, Quat. Sci. Rev., 30, 3109–3123, https://doi.org/10.1016/j.quascirev.2011.07.010, 2011.

820 Weckström, K., Roche, B. R., Miettinen, A., Krawczyk, D., Limoges, A., Juggins, S., Ribeiro, S., and Heikkilä, M.: Improving the paleoceanographic proxy tool kit – On the biogeography and ecology of the sea ice-associated species Fragilariopsis oceanica, Fragilariopsis reginae-jahniae and Fossula arctica in the northern North Atlantic, Mar. Micropaleontol., 157, https://doi.org/10.1016/j.marmicro.2020.101860, 2020.

Wickham, H., François, R., Henry, L., and Müller, K.: dplyr: a grammar of data manipulation. R package version 1.0.8,

825   https://cran.r-project.org/web/packages/dplyr/index.html, 2022.

Zeileis, A., Grothendieck, G., Ryan, J. A., Ulrich, J. M., and Andrews, F.: zoo: S3 Infrastructure for Regular and Irregular

Time Series (Z's Ordered Observations). R package version 1.8-10, https://cran.r-project.org/web/packages/zoo/index.html,

2022.

Zhong, Y., Jahn, A., Miller, G. H., and Geirsdottir, A.: Asymmetric cooling of the Atlantic and Pacific Arctic during the past

830   two   millennia: A   dual   observation-modeling   study,   Geophys.   Res.   Lett.,   45,   12,497-12,505,

https://doi.org/10.1029/2018GL079447, 2018.